MICHIGAN STATE
UNIVERSITY

National Superconducting Cyclotron Laboratory

LIQUID-GAS PHASE TRANSITION IN NUCLEAR MULTIFRAGMENTATION

Submitted to Adv. Nucl. Phys.

S. DAS GUPTA, A.Z. MEKJIAN and M.B. TSANG

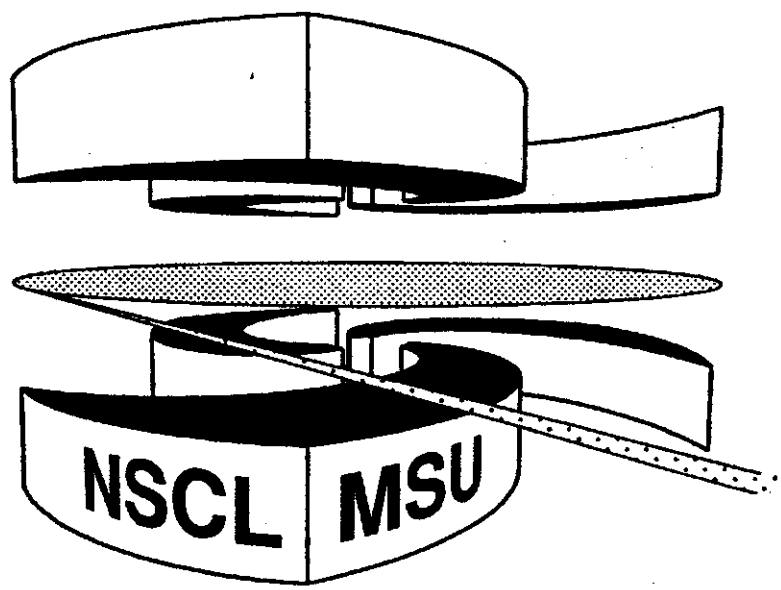

MSUCL-1178 **OCTOBER 2000**

Liquid-gas Phase Transition in Nuclear Multifragmentation

S. Das Gupta[1], A. Z. Mekjian[2] and M. B. Tsang[3]
[1]Physics Dept., McGill University, 3600 University Street, Montreal, Canada H3A 2T8
[2]Physics Dept., Rutgers University, Piscataway, New Jersey 08854, USA
[3]National Superconducting Cyclotron Laboratory, Michigan State University, East Lansing, Michigan 48824, USA
(October 5, 2000)

Abstract

The equation of state of nuclear matter suggests that at suitable beam energies the disassembling hot system formed in heavy ion collisions will pass through a liquid-gas coexistence region. Searching for the signatures of the phase transition has been a very important focal point of experimental endeavours in heavy-ion collisions, in the last fifteen years. Simultaneously theoretical models have been developed to provide information about the equation of state and reaction mechanisms consistent with the experimental observables. This article is a review of this endeavour.

I. INTRODUCTION

Heavy-ion collisions allow one to pump energy into a nuclear system. In central collisions of equal size nuclei one can also create a significant amount of compression using high energy nuclear beams. The possibility of studying nuclei far from normal conditions raises the question: can we study phase transitions in nuclei similar, for instance, to the way, one can study phase transition in water? This is the subject of the present article.

Two important phase transitions are being studied using heavy-ion collisions from medium to very high energies. One phase transition occurs at densities that are subnormal and at temperatures of a few MeV (1 MeV$\approx 10^{10}K$). Nuclei at normal density and zero temperature behave like Fermi liquids so that this transition is a liquid to gas phase transition. The second phase transition of current interest is expected at a much higher temperature ($\approx$150 MeV) and at a much higher density (several times normal density) and will be the subject of intense experimental investigation at the Relativistic Heavy Ion Collider (RHIC) and at CERN in the coming decade. There one expects to see transition from hadronic matter to a quark-gluon plasma. In very high energy collisions many new particles are created. This is a domain very much beyond the limits of non-relativistic quantum mechanics with conservation of particles. Thus, we will not treat this phenomenon at all. Instead at an energy scale of tens of MeV, we should be able to stretch or compress pieces of nuclear matter and we expect to see Van der Waals type of behavior. As a Van der Waals gas is considered to be a classic example of a liquid-gas phase transition, we have a situation similar to that in condensed matter physics.

Unfortunately, the experimental conditions in the nuclear physics case are quite severe. The collisions which produce different phases of nuclear matter are over in 10^{-22} seconds. Thus, we can not keep matter in an "abnormal" state long enough to study the properties. Furthermore, the detectors measure only the products of these collisions where all the final products are in normal states. We have to extrapolate from the end products to what happened during disassembly. This is a difficult task which complicates confirmation of theoretical predictions.

This article is written so that it is suitable for nuclear physicists not specialised in the area of heavy-ion collisions. We hope it is also accessible to non nuclear physicists since the ideas are quite general and well-known from statistical physics. We hope practising heavy-ion collision physicists will also find this a useful reference. The plan of the article is as follows. Section II deals with early theoretical discussions which showed that well established models predict that during disassembly after heavy-ion collisions bulk matter will enter liquid-gas coexistence region provided the beam energies are suitably chosen. In Section III an experimental overview is provided. Sections IV to IX bring us in contact with some experimental results. Here we show, for example, how estimates of temperature or freeze-out density are extracted from experiments. Sections X to XXII are primarily theoretical. We introduce and develop some models; some we simply sketch without providing all the details, as that would make the article extremely long.

II. LIQUID GAS PHASE TRANSITION IN NUCLEAR MEAN-FIELD THEORY

Nuclear matter is an idealised system of equal number of neutrons N and protons Z. The system is vary large and the Coulomb interaction between protons is switched off. For light nuclei the Coulomb interaction has a very small effect and N=Z nuclei have the highest binding energy. As nuclei get bigger the Coulomb energy shifts the highest binding energy towards nuclei with N>Z. This brings into play the symmetry energy which is repulsive and is proportional to $(N-Z)^2/(N+Z)$. Stable systems are scarce after mass number A=N+Z>260. Thus no known nuclei approach the limit of nuclear matter. However, extrapolation from known nuclei leads one to deduce that nuclear matter has density $\rho_0 \approx 0.16 fm^{-3}$ and binding energy ≈16 MeV/A. We will choose an Equation of State (EOS) of this idealised nuclear matter to examine if a liquid-gas phase transition can be expected and at what temperature and density.

The following parametrisation, called the Skyrme parametrisation for the interaction potential energy, has been demonstrated [1] to be a good approximation for Hartree-Fock calculations. We take the potential energy density arising from nuclear forces to be

$$v(\rho) = \frac{a}{2}\frac{\rho^2}{\rho_0} + \frac{b}{\sigma+1}\frac{\rho^{\sigma+1}}{\rho_0^{\sigma}} \tag{2.1}$$

Our unit of length is fm and unit of energy is MeV. In the above ρ_0=$0.16 fm^{-3}$, a, b are in MeV, a is attractive, b repulsive and σ is a parameter. The constants should be chosen such that in nuclear matter the minimum energy is obtained at $\rho = \rho_0$ with energy E/A=-16 MeV. This fixes two of the three parameters and the third can be obtained by the compressibility coefficient (nuclear physics has its own unique definition of compressibility coefficient $k\partial p/\partial\rho$ at ρ_0). The Skyrme parametrisation is simple enough that we will write down all the relevant formulae. From Eq.(2.1) the energy per particle as a function of density ρ at zero temperature is given by

$$\frac{E}{A}(\rho) = \frac{a}{2}\frac{\rho}{\rho_0} + \frac{b}{\sigma+1}(\frac{\rho}{\rho_0})^{\sigma} + 22.135(\frac{\rho}{\rho_0})^{2/3} \tag{2.2}$$

In Eq.(2.2) the last term on the right hand side is the zero-temperature Fermi-gas value for kinetic energy. The pressure due to the interaction at zero or any temperature is

$$p = [\frac{a}{2}\frac{\rho}{\rho_0} + \frac{\sigma b}{\sigma+1}(\frac{\rho}{\rho_0})^{\sigma}] \times \rho \tag{2.3}$$

The condition that E/A minimise at $\rho/\rho_0 = 1$ gives

$$\frac{a}{2} + \frac{b\sigma}{\sigma+1} + (2/3) \times 22.135 = 0 \tag{2.4}$$

The condition that E/A is -16 MeV at ρ_0 gives

$$-16 = \frac{a}{2} + \frac{b}{\sigma+1} + 22.135 \tag{2.5}$$

Lastly, compressibility is given by

$$k = 9 \times (a + \sigma b + \frac{p_F^2}{3m}) \tag{2.6}$$

The EOS for the Skyrme parametrisation with a=-356.8 MeV, b=303.9 MeV and σ=7/6 (this gives k = 201MeV) is shown in Fig. 1. In the figure isotherms are drawn for various temperatures (10, 12, 14, 15, 15.64 and 17 MeV). The pressure contributed by kinetic energy was calculated in the finite temperature Fermi-gas model. The similarity with Van der Waals EOS is obvious; for a more quantitative comparison we refer to Jaqaman et. al [2]. With the parameters chosen here the critical temperature is 15.64 MeV. The spinodal region ($\partial p/\partial \rho < 0$) can be seen clearly. The coexistence curve which is shown in the figure is obtained using a Maxwell construction [3].

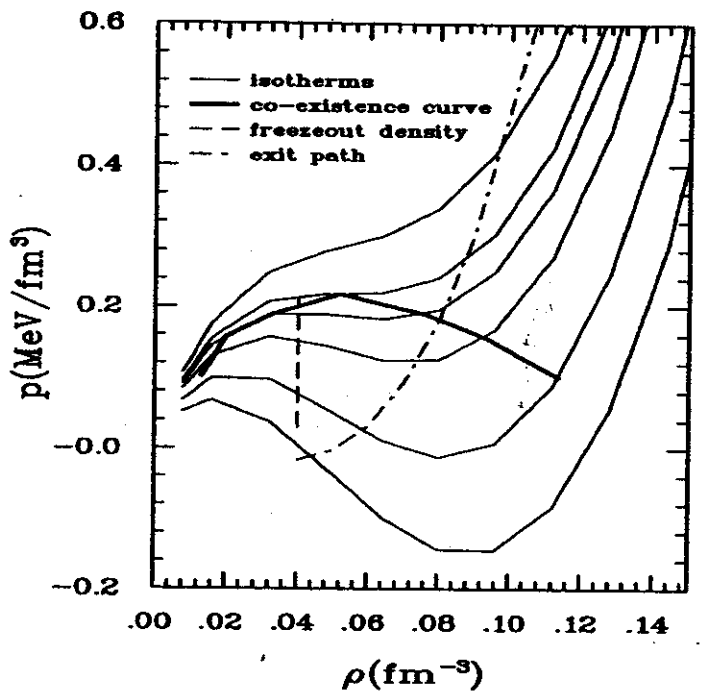

Fig. 1. Nuclear matter equation of state with Skyrme interaction with compressibility 201 MeV. In ascending order the isothermals are at temperatures 10, 12, 14, 15, 15.64 (critical isotherm) and 17 MeV. The coexistence curve obtained from a Maxwell construction is shown. The vertical line is drawn at assumed freeze-out density 0.04 fm^{-3}. The dot-dash line is obtained by assuming that the excited system expands isentropically (see Fig.2). This is an idealisation.

We now describe how in heavy-ion collisions one will sweep across the $p - \rho$ plane. In heavy-ion collisions one distinguishes between spectators and participants. Imagine two equal ions colliding at zero impact parameter. Some highly excited nucleons are emitted first. The other nucleons are called participants because each nucleon will collide with at least one nucleon in its path if all nucleons are assumed to move in straight line paths. In peripheral collisions where the impact parameters are non-zero, nucleons outside the overlapping zone would not have collided with nucleons from the other nucleus. These "non-interacting" nucleons are defined as spectators. For the same beam energy much more energy is pumped

into the participating zone. There will even be compression in this zone if the excitation is very high. Spectators are only mildly excited. They are excited for many reasons: highly non-spherical shapes, unfavourable N/Z ratios, migration from participants etc.. In general, spectators should have little compression. Both central and peripheral collisions have been studied to find signals of phase transitions.

Imagine then, as a result of heavy-ion collisions, nuclear matter has been excited to a high temperature, with or without compression. Looking at Fig. 1 we see that the pressure will be positive and matter will begin to expand [4–6]. The exit path is hard to guess but the simplest expectation supported by transport models is that it is approximately isentropic in the beginning part of the expansion. However, if the system reaches the spinodal region, the mean-field description is inappropriate and the system is expected to break up into chunks. In Fig. 1 we have nonetheless followed the isentropic trajectory. Expansion continues till it reaches a freeze-out volume, a theoretical idealisation. Once the freeze-out volume is reached there is no exchange of matter between different fragments. Since the fragments are still hot, they will get rid of their excitation by evaporation (sequential two body decays [7,8]) before they reach the detector. The freeze-out density is significantly lower than the normal density. It is probably not as low as one-tenth the normal density because interactions between fragments (except for Coulomb forces) will cease well before that. The freeze-out density is often a parameter in the theory adjusted to get the best fit and is model dependent. The 'best' choice seems to be always less than half the normal density. In Fig. 1 we have shown this arbitrarily to be $\rho_{fr} = 0.04 fm^{-3}$, that is, one-quarter of normal nuclear density.

Normally, the EOS is drawn with isotherms but some additional insight can be gained by looking at isentrops [6]. For this we refer to Fig. 2 where we have drawn, for the same Skyrme interaction, $\frac{E}{A}(\rho)$ and $p(\rho)$ but now for constant entropy instead of constant temperature.

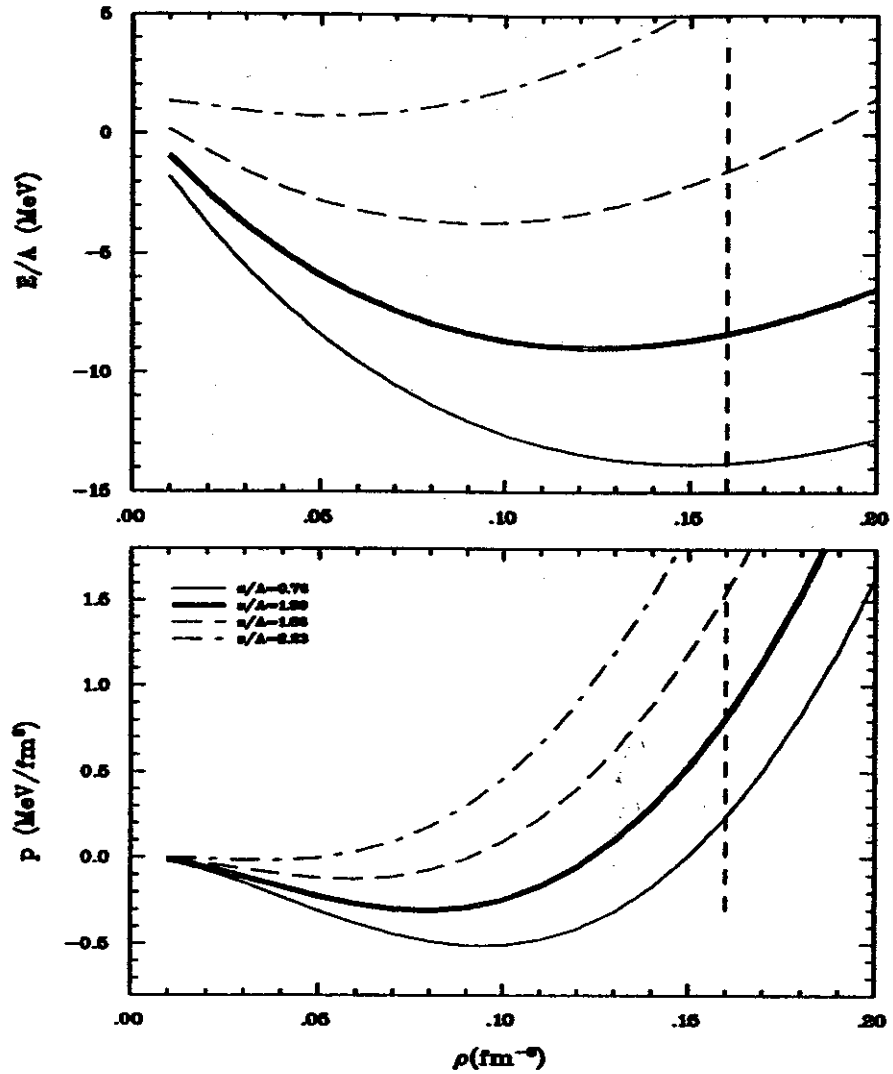

Fig.2. For the same Skyrme interaction as used in Fig.1, we draw $\frac{E}{A}(\rho)$ and $p(\rho)$ but now for fixed entropy rather than fixed temperature. The vertical dashed line is along normal nuclear density. We consider disassembly of an excited spectator. If the system starts from $E/A \approx -2$MeV (entropy 1.86 per particle), the initial pressure is positive and it begins to expand (in this idealisation) along the isentrop. The thermal E/A will fall, and to compensate, collective velocity will develop. This collective velocity will take the system beyond the minimum of E/A and drive it to the region of spinodal instability. For small excitation energy and entropy(0.76) the system starts with positive pressure but does not attain enough collective velocity to reach the spinodal region. It will de-excite by sequential decay.

Imagine then an excited spectator is formed at normal density indicated by the vertical dashed line. Let us focus on two isentrops, S/A=1.86 and S/A=0.76. In the first case the system starts with $E/A \approx -2$ MeV and positive pressure. It will begin to expand; the value of "thermal" E/A as it expands along the isentrop, drops. For conservation of energy it must then develop a collective flow. This collective flow will take it beyond the minimum

of E/A and drives it to the spinodal region. For the isentrop with value 0.76, even though it starts with positive pressure, it does not gain enough collective energy to drive it to the spinodal region. It will therefore oscillate around zero pressure and has to de-excite by other means (two-body decay [7]). The intermediate case with S/A= 1.39 just makes it to the spinodal region.

It is also clear both from Fig. 1 and Fig. 2 that if the starting point is too high (i.e., too much excitation energy) the system will entirely miss the liquid region and probe only the gas region at the time of dissociation. This was the case at Bevalac [9] (incident energy in GeV) where the goal of studying heavy-ion reactions was quite different.

While mean-field theory, as described above, easily leads to a liquid-gas phase transition picture, one clearly needs to go much beyond. There is hardly any observable that one can calculate using mean-field theory alone. Most common experimental observables are the clusters, their compositions, their excitations, velocities etc. Mean-field theory does not give these values although it suggests that the system must break up because of spinodal instability. However, with the Maxwell construction obtained from the mean-field EOS one can draw a coexistence curve (Fig. 1) and this has experimental relevance. As we will describe in much greater detail later, one may measure the caloric curve [10] defined as T vs. E^*/A in heavy ion experiments. The experiment gives a measure of the specific heat, dE^*/dT in the vicinity of temperature 5 MeV. Indeed many models (to be described in later sections) produce a peak in the specific heat at about this temperature. The peak is reminiscent of the crossing of the coexistence curve [11]. These models are also able to calculate many other observables with reasonable success. Let us refer to Fig.1 to see where we would expect to see the peak in mean-field theory. If we consider the freeze-out density to be $0.04fm^{-3}$, the intersection of the $0.04fm^{-3}$ line and the coexistence curve suggests a temperature of about 15 MeV. This "boiling" temperature will come down if a lower freeze-out density is used but even at one tenth the normal density the boiling temperature is still 12 MeV. Since we have used nuclear matter theory, the temperature is expected to be lower due to finite particle number and Coulomb interaction. In ref [2] and later in [12], the effect of finite particle number was estimated to be significant. In addition we must remember that mean-field theories normally overestimate the critical temperature. For example, in the Ising model, this overestimation is about 50 per cent [13]. In mean-field Thomas-Fermi theory that includes the Coulomb interaction De *et. al.* [14] find the peak in specific heat at 10 MeV for ^{150}Sm. Without the Coulomb interaction, in bulk matter with the same isospin asymmetry as ^{150}Sm, the peak is located at 13 MeV. As will be described in greater detail later, both experimental data and more realistic models point to much lower temperature. Thus in mean-field theory interesting things seem to happen at too high a temperature.

III. EXPERIMENTAL OVERVIEW

Experimentally the following features are well known. At excitation energy $\epsilon \approx 1$ MeV/nucleon, successive emissions of particles by evaporation of the compound nucleus or its fission are the basic deexcitation mechanisms. The picture can be justified by saying that there is enough time between successive emissions so that the nucleus can relax ($\tau_{re} \approx 2R/c_s$) to a new equilibrium state where R is the radius of the compound nucleus and c_s is the velocity of sound. At $\epsilon \approx 3$ MeV/nucleon, the time interval between successive

emissions is comparable with τ_{re}. At excitation energy comparable to binding energy $\epsilon \approx 8$ MeV/nucleon the very existence of a long-lived compound nucleus is unlikely which leads to the scenario of an explosion-like process involving the whole nucleus. This will lead to multiple emission of nuclear fragments of different masses. This is what is called "multifragmentation" where 'multi' is more than two. Associated with multifragmentation is a term Intermediate Mass Fragment (IMF) that we will use often. This refers to particles with charge Z between 3 and 20 to 30. The lower charge limit is set to 3 because of exceptional binding of the alpha particle. The upper limit is set not to include fission like fragments; if the nucleus broke up into several chunks in the spinodal region, we could expect some of them to be IMF's. In the mean-field scenario described earlier, multifragmentation is associated with the co-existence region. Thus, it is considered to be the most promising experimental observable to study the liquid-gas phase transition in nuclear matter. However, while phase transition signals will always be weakened by finite particle number effects, multifragmentation is usually found at the appropriate energy and occurs in nuclear collisions even when the thermodynamic limit is not reached. Thus multifragmentation is a more general process than phase transition.

In the co-existence region, light particles such as neutrons, hydrogen isotopes (p, d, t) and helium isotopes (^{3}He, ^{4}He, ^{6}He) are considered as gas while the IMF's are treated as droplet forms of the liquid. In collisions where larger residues remain, they are the liquid remnants from the original colliding nuclei. Since nuclei are two-component systems consisting of neutrons and protons, the isotopic contents of the gas and the liquid phase will be different. This is specially so when bound nuclei of smaller sizes are usually found along the valley of stability and have nearly equal number of protons and neutrons. Thus if the initial collisions consist of heavy nuclei which have more neutrons than protons, one would expect the excess neutrons to diffuse out to the gas region resulting in a neutron enriched nucleon gas. This has already been seen in experiments and will be discussed later. Thus a preliminary glimpse of the phase transition in nuclei suggests a much richer structure than what has been implied by nuclear matter alone.

Multifragmentation was seen in high-energy proton-nucleus collisions [15–18] before systematic studies were undertaken in nucleus-nucleus collisions. For a proton incident on a nucleus the picture is as follows. Shortly after the collision between the proton and the target nucleus, several prompt nucleons leave the system and carry off much of the energy of the collision. At low incident proton energies only remnants near the mass of the target are produced. For incident proton energies around 0.5 GeV, the system undergoes fission leaving two large fragments. When the incident proton energies are between 1.0 GeV and 10 GeV, the cross-section for multifragmentation rises by an order of magnitude. At energies above 20 GeV the cross-section becomes independent of energy, reaching the limiting fragmentation region.

Systematic studies of multifragmentation have been undertaken using heavy-ion beams since the mid eighties, when these beams became routinely available and large detection arrays were built. The production of fragments from central collisions reaches a maximum around 100A MeV. In the following section we will examine various aspects of the multifragmentation process, which may be employed to signal the liquid-gas phase transition.

IV. EVENT SELECTION

Most early multifragmentation experiments are inclusive measurements [15–20], i.e. particles are identified with no requirements that other particles from the same event should be detected in coincidence. These types of experiments do not provide information about the collision dynamics or properties of the emission sources from the nuclear reaction. Since multifragmentation of spectators, produced in peripheral collisions has different characteristics from fragments emitted from the participant zone formed in central collisions, it is important that the emission sources be identified. There are both advantages and disadvantages of using central or peripheral collisions to find the signals of phase transition. In this section, the methods used to select central and peripheral collisions will be discussed.

A. Central Collisions

In central collisions, the excitation energy pumped into the participant zone is higher and the source characteristics, i.e. selection of a single source, can be accomplished easily with large detector arrays which provide nearly 4π angular coverage. Intuitively, one expects more particles to be produced in violent or central collisions than peripheral collisions. Thus the number of emitted particles can be related to the collision geometry and the simplest observable is the number of charged particles detected, N_c. There are variations of the observable N_c, such as the hydrogen multiplicity, N_1 or light charge particle multiplicity, N_{LCP}. All these observables work reasonably well in distinguishing central collisions with small impact parameters from peripheral collisions [21]. However, the neutron multiplicity, N_n [22] and the IMF multiplicity, N_{IMF} [23] do not work as well. Aside from multiplicities, there are other observables such as the mid-rapidity charge, Z_y, [24] and the total transverse kinetic energy, E_t, of the identified particles [25], which can be used as an impact parameter filter. Z_y is the summed charge of particles with rapidity between that of the target and projectile. This quantity reflects properties of the participant zone. The total transverse energy is defined as $E_t = \sum_i E_i sin^2\theta_i = \sum_i (p_i sin\theta_i)^2/2m_i$ where E_i, p_i, and θ_i denote the kinetic energy, momentum and emission angle of particle i with respect to the beam axis.

The most common way to relate an experimental observable to the impact parameter is to assume a monotonic relationship between the observable and the impact parameter [26,21]. In general, a reduced impact-parameter scale, $\hat{b}$ which ranges between 0 (head-on collisions) to 1 (glancing collisions), is defined as

$$\hat{b} = b(X)/b_{max} = (\int_X^\infty [dP(X')/dX']dX')^{1/2} \tag{4.1}$$

where $X = N_C, N_1, N_n, N_{IMF}, N_{LCP}, E_t, Z_y, dP(X)/dX$ is the normalized probability distribution for the measured quantity X, and b_{max} is the maximum impact parameter for which particles were detected in the near 4π detection array.

For illustration of the impact parameter determination, the top panel of Fig.3 shows the charged particle multiplicity distribution of the ^{84}Kr induced reaction on ^{197}Au at 35 MeV per nucleon incident energy [27]. The bottom panel shows the relationship between the reduced impact parameter, $\hat{b}$, and N_c with a lower cut of $N_c > 2$ applied in the analysis.

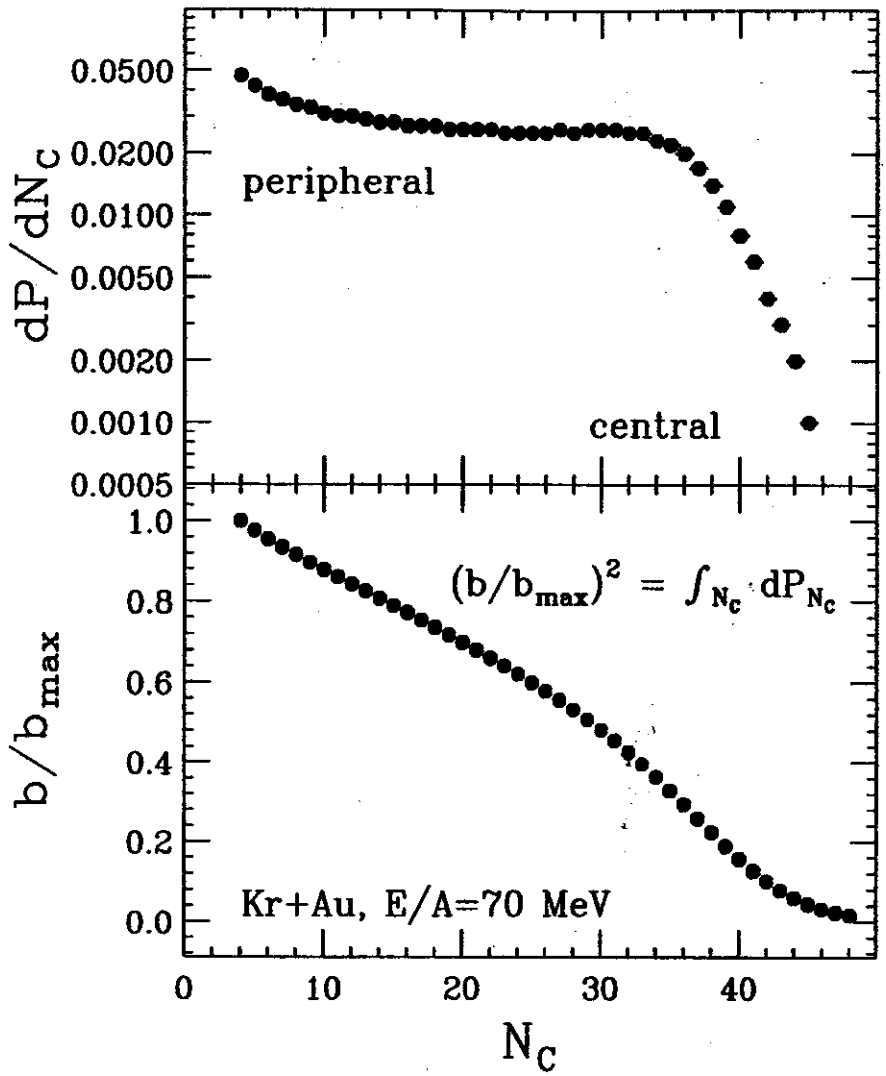

Fig. 3: (Top) Charged particle multiplicity distribution of the ^{84}Kr induced reaction on ^{197}Au at 35 MeV per nucleon incident energy. (Bottom) $\hat{b}$ as a function of N_c [27].

While N_c is the most simple observable to measure the impact parameters, it is not very precise due to fluctuations and geometric efficiencies of the detection device . In cases where the single source from the central collision needs to be better defined or determined, additional constraints are applied. In head-on collisions, the angular momentum transfer is zero and all the emitted particles are emitted isotropically in the azimuthal angle [28]. Thus additional constraints on central collisions can be placed by requiring the detected particles to have isotropic emission pattern. Other constraints include requiring the total charge detected to be a substantial fraction of that of the initial system [29], the ratio of total transverse momentum to longitudinal kinetic energy or by requiring the velocity of the emitted particles to be about half of the center of mass velocity [24,30]. Obviously, each additional constraint reduces the number of events available for analysis. Too many constraints may reduce the data to the extreme tails of the distributions where large fluctuations of the observable become a problem.

During the compression stage, pressure in the central region causes the participant zone to expand [31]. Thus part of the available energy in central collision is converted to collective energy such as radial flow which expands outward, or transverse flow caused by the spectators being pushed by the participant region to the side, and the squeeze-out of nucleons from the participant region perpendicular to the reaction plane due to blocking by the spectators [32]. Clearly, all these collective motions strongly affect the signals of the phase-transition observed in central collisions and reduce the amount of excitation energy available for heating up the system. They must be understood and taken into account in the study of phase transition.

B. Peripheral Collisions

Theoretically, spectators should be less affected by the effects of collective motion than the participants. The collision kinematics focus the emitted fragments from the projectile to the forward direction in the laboratory. These fragments are generally detected with spectrometers or detectors placed at forward angles and the charges, velocities etc. are identified. The decay of a projectile spectator is easier to study experimentally than the target spectator which is emitted backward with very low energy in the laboratory frame.

Unlike central collisions, the impact parameter is strongly correlated with the size of the source in peripheral collisions. Thus the size of the projectile-like residue such as the charge, Z_{PLF}, provides some indication of the impact parameter [33]. In the case where most of the projectiles fragment into many small pieces, the quantity Z_{bound} defined as the sum of atomic numbers Z_i of all fragments with $Z_i \geq 2$ has been found to be a good measure for impact parameter [34]. It represents the charge of the spectator system reduced by the number of hydrogen isotopes emitted during its decay and thus, it is the complement of the hydrogen multiplicity, N_1. In an experiment where both Z_{bound} was measured by the forward spectrometer and N_c was measured by a 4π array in the reaction of Au+Au at E/A=400 MeV, the two observables are anti-correlated [35]. Thus, like N_c and other observables discussed in previous section, Z_{bound} can be used in eq.(4.1) to provide a quantitative measure of the impact parameter.

V. EVIDENCE FOR NUCLEAR EXPANSION

Around incident energy of 50A MeV, fragment multiplicities increase with the size of the emission source and excitation energy. In examining reactions of Xe on various targets, ^{12}C, ^{27}Al, ^{51}V, ^{nat}Cu, ^{89}Y and ^{197}Au, even though the targets span a range of N/Z from 1.0 to 1.5, a near-universal correlation has been observed between the average number of emitted IMFs, $< N_{IMF} >$, and the charge-particle multiplicity, N_c, for non- central collisions [36]. Fig.4 shows the mean number of IMF detected in the collision of ^{129}Xe+^{197}Au at 50A MeV as a function of the detected charge particle multiplicity, N_c [37]. In the most central collision, N_c >33, the mean number of $< N_{IMF} >$ is 7 but up to 14 IMF fragments have been observed. The large fragment multiplicities cannot be reproduced by the break-up of the hot system at normal nuclear matter density with either the dynamical or statistical models. (Predictions of various statistical models are lower than the data as shown by the

dashed lines, open circles and crosses.) Calculations requiring expansion to less than 1/3 of the normal nuclear matter density is needed to explain the large increase in $< N_{imf} >$ as shown by the solid lines.

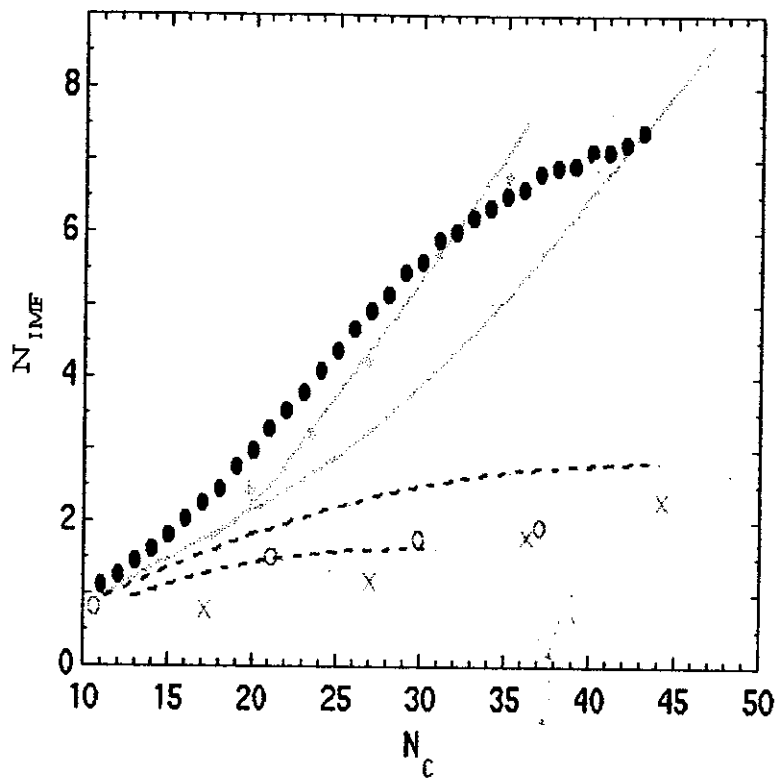

Fig. 4: The mean number of IMF detected N_{IMF} in the collision of ^{129}Xe+^{197}Au at 50A MeV as a function of the detected charge particle multiplicity, N_c. Data are represented by the solid points. The dashed lines, open circles and crosses are data from various statistical models assuming normal nuclear matter density. They all under-predict the number of IMF emitted. The solid lines are calculations from an expanding nuclear system. See [37] for more details about the calculations.

If the hot nuclear system expands, the "radial" component of the velocity should be evidenced in the particle energy spectra. Without the influence of radial expansion, the energy spectra resulting from the collision of a target and projectile at intermediate energy are composed of three isotropically emitting thermal sources corresponding to the projectile-like and target- like spectators in addition to the participant region formed by the overlap of the projectile and target. Instead, the IMF and light particle energy spectra from the central collisions of Au+Au reaction show a shoulder like shape [38,39]. To fit the energy spectra, large radial expansion velocities are required in addition to the three sources [38,39]. Similarly, the mean kinetic and transverse energy of emitted fragments also provide measure of the radial collective velocities when compared to the predictions of thermal models [40–42]. Fig.5 shows a nearly linear relationship between the radial velocities with the incident energy [40]. The plot suggests that 30% to 60% of the available energy is used in the radial expansion. This energy is thus not available for thermal heating of the nuclear matter. Evidence for the "nuclear expansion" of the hot nuclear systems is a necessary but not

sufficient condition for the occurrence of a liquid-gas phase transition.

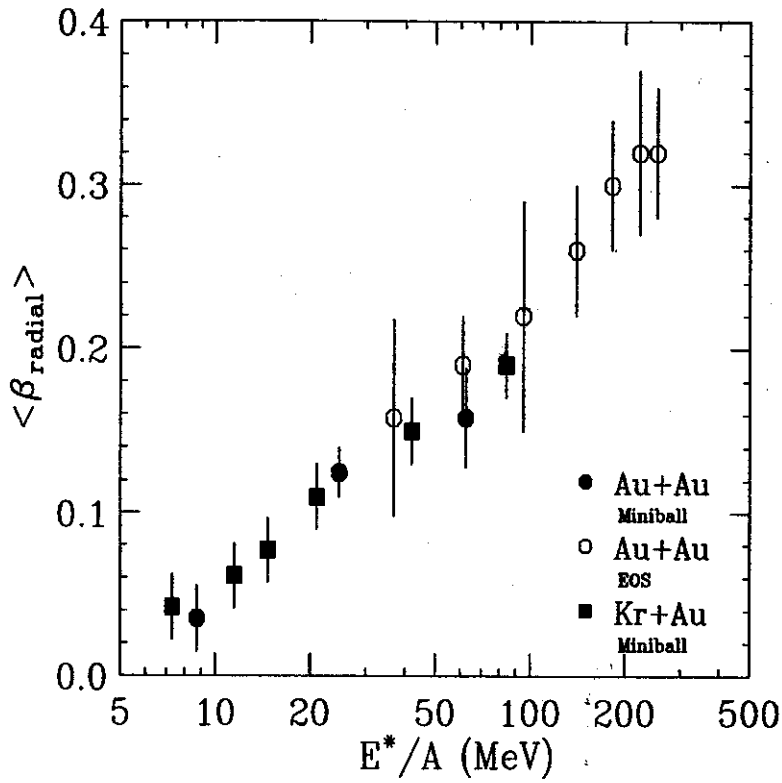

Fig. 5: Systematics of average radial velocity as a function of incident energy for various systems [40].

VI. SPACE-TIME DETERMINATION

The average radial velocity plotted in Fig.5 indicates that the nuclear expansion occurs in a rather short time (10^{-22} second). As a result of the fast expansion, the density of the reaction zone is below normal nuclear matter density. Information about the space-time evolution of the reaction zone can be obtained via intensity interferometry. The principle behind such experiments is similar to the intensity interferometry [43] employed to determine the radius of stars, where both singles (Y_i) and coincident (Y_{12}) yields of photons from the same source (star) are measured. Intuitively, one expects the correlation to be small if the source size is large and a large correlation from a small source. In nuclear physics, particles are detected instead of photons. A correlation function constructed from these yields is defined as, $1 + R(p_1, p_2) = Y_{12}(p_{12})/(Y_1(p_1)Y_2(p_2))$ where p_i is the laboratory momentum of particle i. At large relative momenta where the final interaction is negligible, $R(p_1, p_2)$ should be zero. Unlike astronomy where the space-time evolution of stars is slow, the time scale involved in nuclear physics is very short. Thus there are ambiguities in determining the size and time-scale of nuclear reactions using intensity interferometry, because a small source emitting over a long period of time behaves like a large source emitting over a short period of time [44].

The space-time information of the emitting source can be obtained by measuring the correlation function. An example of the fragment-fragment correlation from the Ar+Au reaction at E/A=50 MeV is shown in Fig.6 [45] as a function of the reduced velocity, $v_{red} = v_{rel}/\sqrt{(Z_1 + Z_2)}$ where v_{rel} is the relative velocity between fragment 1 and 2. The use of v_{red} allows summing over different combinations of fragment-fragment correlations. Basic features of the correlation functions for different particle pairs depend on details of the final state interaction between the two particles. For intermediate mass-fragments, the most important interaction is the Coulomb interaction between the particles as shown by the suppression of the correlation functions at small v_{red}. However, if the fragments are emitted in the vicinity of a heavy reaction residue, the Coulomb interaction with the residue may not be neglected [46]. This space-time ambiguity is illustrated by the calculations shown as lines in Fig.6 [45].

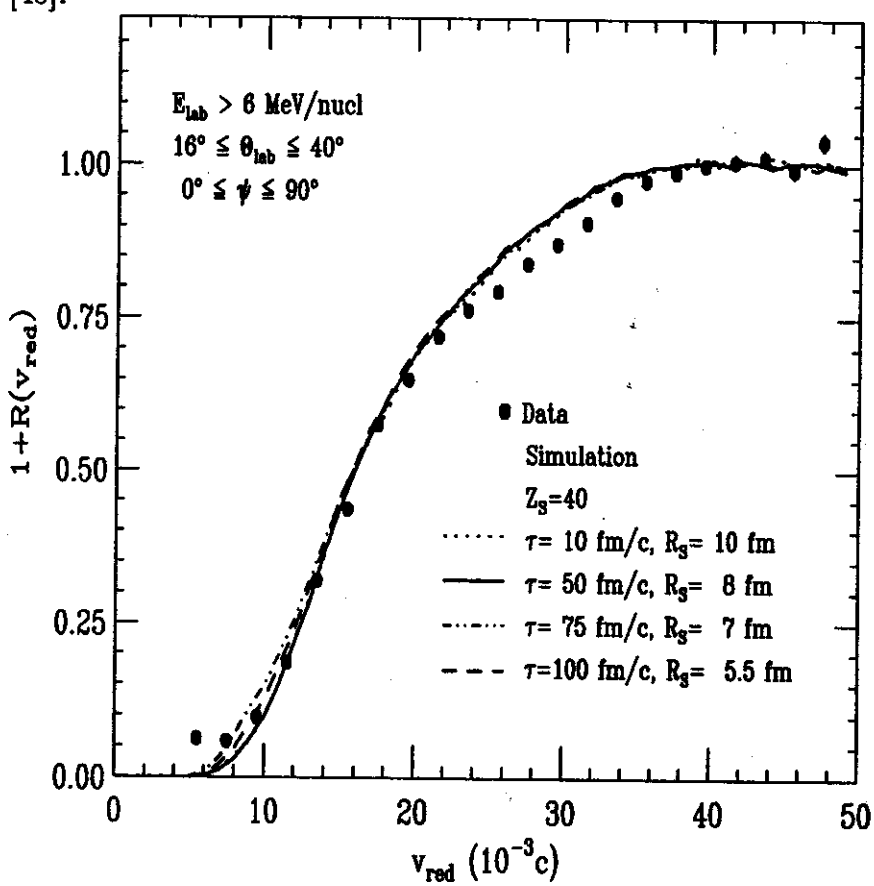

Fig. 6: The fragment-fragment correlation from the Ar+Au reaction at E/A=50 MeV is shown as a function of the reduced velocity, $v_{red} = v_{rel}/\sqrt{(Z1 + Z2)}$ where v_{rel} is the relative velocity between fragment 1 and 2 [45]. The lines are Monte Carlo simulations of many body Coulomb trajectory calculations of fragments emitted from a spherical source of radius R_s and lifetime τ.

The calculations are Monte Carlo simulations of many body Coulomb trajectory calculations of fragments emitted from a spherical source of radius R_s and lifetime τ. The data are

equally well described by calculations using four different combinations of R_s and τ as shown in the figure. Even with this ambiguity, the "valley" exhibited at low v_{red} provides some measure of the space-time extent of the source. As the energy increases, the width of this "valley" increases suggesting emission from a smaller and may be a faster source. In order to get more definite results about the emission time, information about the source size must be obtained independently. Such information is most commonly extracted by comparing predictions with data and thus is model dependent. For example, assuming that the source sizes can be obtained from the linear momentum transferred to the system, one can obtain the emission time from fragment-fragment correlation functions. The left panel of fig.7 shows the dependence of mean emission time as a function of incident energy for the system Kr+Nb [47]. Above 55 MeV per nucleon, multifragmentation seems to occur in a time scale that saturates at ≈125 fm/c. The result is consistent with breakup of a fragmenting source at low density including those driven by Coulomb instabilities as in the Au+Au reaction at E/A=35 MeV [42]. In the latter experiment, the source size was obtained by comparing various experimental observables to the prediction of the statistical multifragmentation model. Recent analysis of the IMF correlation functions from high energy hadron induced multifragmentation suggests the saturation time occurs at much shorter time scale (<100 fm/c) as shown in the right panel of fig. 7 [48]. Considering the space-time ambiguity and model dependence in extracting the time information, the correlation analysis is probably not reliable in extracting a time scale less than 50 fm/c.

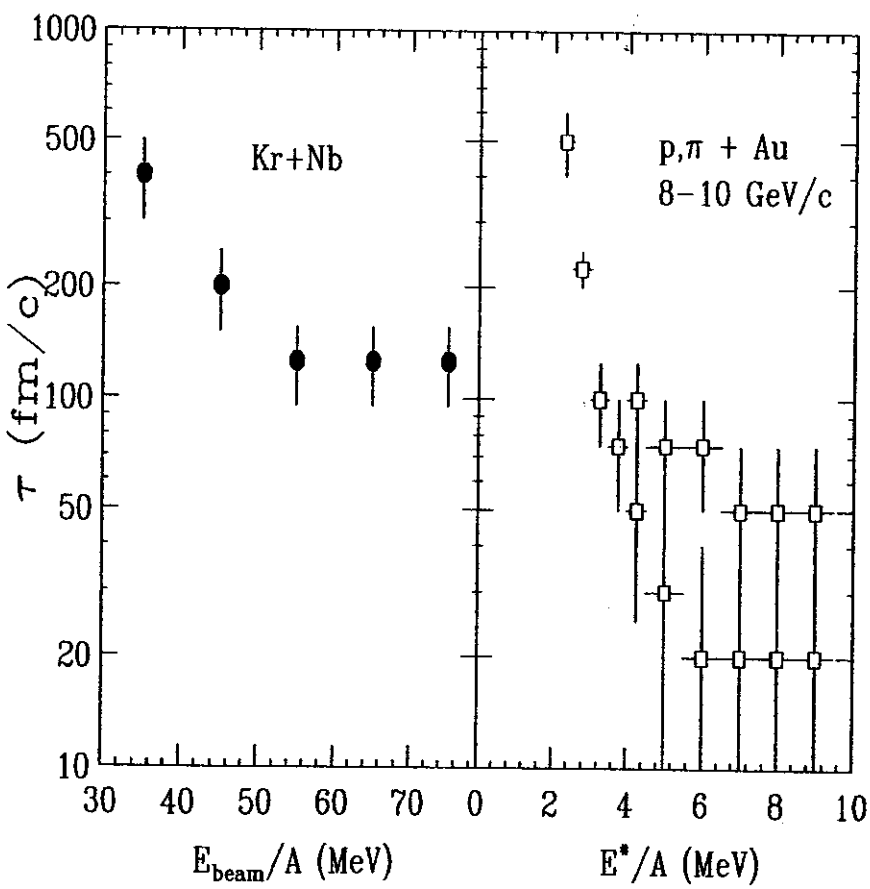

Fig. 7: Dependence of mean emission time as a function of incident energy for the system Kr+Nb [47] (Left panel) and as a function of excitation energy for hadron induced multifragmentation (right panel) [48].

Without precise time information, quantitative measurements of freeze-out densities have been difficult to obtain, since the density is quite sensitive to the emission time and volume of the source. Assuming zero lifetime, the density or source sizes can be obtained from light charged particle correlation measurements [49–51]. The left panel of Fig.8 shows the radii extracted for different reactions using the p-p correlation as a function of the proton velocity normalized by the beam velocity. The middle data set with lots of data points are experimental results from the ^{16}O and ^{14}N induced reaction on Au. The solid diamonds and solid circles are radii extracted from the ^{40}Ar induced reaction on Au and ^{3}He induced reaction on Ag, respectively. The dot-dashed and the dash lines are scaled from the solid lines by the radii of the projectile. At high velocity where the protons originate from the projectile, the scaled predictions agree with the data very well, suggesting that the method of using p-p correlations to extract source size information is consistent within the same method.

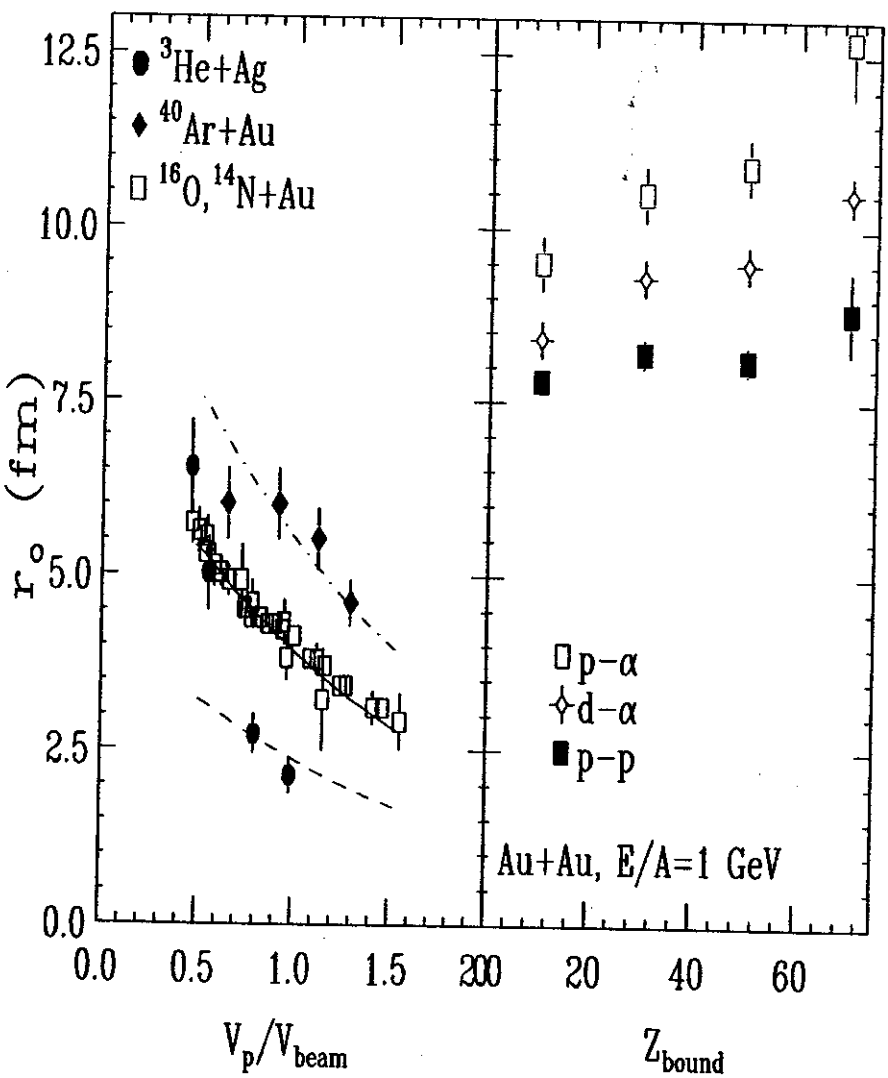

Fig. 8: This shows the radii extracted for different reactions using the p-p correlation as a function of the proton velocity normalized by the beam velocity. The open symbols are radii extracted from ^{16}O and ^{14}N induced reactions on Au. The solid line is the interpolation of this set of data. The solid diamonds and solid circles are radii extracted from the ^{40}Ar induced reaction on Au and ^{3}He induced reaction on Ag, respectively. The dot-dashed and the dash lines are scaled from the solid lines with the radii of the projectile [50]. The right panel shows the radii deduced from the p-p, p-α, d-α correlations as a function of Z_{bound} for the projectile fragmentation of Au+Au at E/A=1000 MeV [51].

The right panel of Fig.8 shows the radii deduced from the p-p [solid squares], p-α [open stars], d-α [open squares] correlations as a function of Z_{bound} for the projectile decay of Au+Au collisions at E/A=1 GeV. The radii obtained from the p-p correlation are smaller than the radii obtained from p-α correlations which are in turn smaller than the radii obtained from d-α correlations. There is no logical explanation for such an observation. The inconsistencies of the measurements, regarding the different radius values obtained from different particle correlations, illustrate the present experimental difficulties in extracting the precise values of the freeze-out densities since the analysis is highly model dependent. Other methods, such as comparing IMF multiplicities or mean kinetic energies with statistical models have been employed to determine the source sizes [42]. Independent of different analysis methods, densities lower than 1/3 of the normal nuclear matter density provide the best agreement with the data. Consistent with such a conjecture, models that assume normal nuclear matter density underpredict the fragment multiplicities [37,52–54].

Considering the complexities of the issue, the available experimental data suggest a time scale for the multifragmentation process of the order of 100 fm/c and density values of less than a third of the normal nuclear matter density. Obviously, it is desirable to have more exact values. Further experimental work and better understanding of the reaction mechanisms in the coming years will allow more precise measurements in this area.

VII. TEMPERATURE MEASUREMENTS

A. Kinetic Temperatures

How valid is the concept of temperature in heavy ion reactions? Long before intermediate energy collisions which are best described by multifragmenation mechanisms, the concept of temperature was being used routinely to describe heavy ion collisions at Bevalac (see for example [16]). In cascade [55] or transport calculations [56] one can follow in microscopic models how the original ordered motion of the beam gets dispersed into a Maxwell-Boltzmann distribution through two-body collisions. In the Purdue experiment of proton on Xe [18], the high energy tails of the kinetic energy spectra provide evidence that the fragments originate from a common remnant system somewhat lighter than the target which disassembles simultaneously into a multibody final system. Theoretically, the slopes of the particle kinetic energy spectra assuming a Maxwellian distribution, should be sensitive to the initial temperature.

$$\frac{d^2\sigma}{dEd\Omega} = N_0(E - V_c)^{1/2}.\exp(-E_*/T_{kin}) \qquad (7.1)$$

where $E_s = E - V_c + E_0 - 2[E_0(E - V_c)]^{1/2}\cos(\theta)$ Here N_0 is a normalization constant; E and m are the energy and mass of the emitted particle; θ is the detection angle relative to the incident beam; T_{kin} is the slope or kinetic temperature; $E_0 = mv_0^2/2$; and V_c corrects for the Coulomb repulsion from the target residue. As discussed earlier, collective motions complicate the energy spectra. Furthermore, fluctuations in Coulomb barriers, sequential feedings from higher-lying states [57], Fermi motion [58] and pre-equilibrium emissions all contribute to the complications associated with extracting emission temperatures from the energy spectra.

B. Excited state temperature

To circumvent some of these problems, other thermometers, which are less sensitive to the collective motion, have been sought. Thermometers based upon the relative populations of excited states of emitted light particles have been used quite extensively in extracting the temperatures of the hot nuclear systems.

$$T = \frac{E_1 - E_2}{ln(a'Y_1/Y_2)} \tag{7.2}$$

Here $a' = (2J_2 + 1)/(2J_1 + 1)$, E_i is the excitation energy, Y_i is the measured yield and J_i is the spin of the state i. To minimize the influence of sequential decays, nuclei with levels that are widely separated are often chosen [59]. One of the most commonly used nuclei is the unstable ^{5}Li isotope. The ground state $3/2^+$ decays to p and α particles while the 16.66 MeV $3/2^+$ excited state decays into d and ^{3}He particles. Statistical models incorporating the effect of sequential decays suggest that temperatures up to 6 MeV should be obtainable with this nucleus based on the excited states population [60]. Other nuclei include α particles, ^{10}B and ^{8}Be which all have relatively widely separated states. Even though the ground state and first excited state of the alpha particle are separated by 20.1 MeV, a substantial part of the measured ground state alpha yields can be attributed to sequential decays from heavy nuclei due to the unusual binding energy of the alpha particles. The consistency of the method is normally checked by measuring the temperatures of several nuclei.

C. Isotope temperature

Another thermometer, T_{iso}, which utilizes the yield ratios of two pairs of isotopes have been under intense study in the past few years [61,62]. If chemical and thermal equilibrium are achieved, in the limit of the Grand Canonical Ensemble, one can obtain the isotope temperature information from a double isotope ratio defined by

$$T = \frac{B}{ln(a(Y_1/Y_2)/(Y_3/Y_4))} \tag{7.3}$$

where Y_1, Y_2 are the yields of one isotope pair and Y_3, Y_4 is another isotope pair. To cancel the nucleon chemical potential terms, the mass number differences of isotope pair (1,2) must be the same as the mass number differences of isotope pair (3,4); B is the binding energy difference, $B = BE_1 + BE_2 - (BE_3 + BE_4)$; a contains the statistical weighting factor. This

equation assumes that the sequential decay corrections to the yields are negligible. This assumption is rather problematic as the experimental measured yields are "cold" fragments containing contributions from the decays of many excited nuclei. In experiments where a large number of isotope yields are measured such as the proton induced reaction on Xe [18], thousands of T_{iso} values can be extracted [63] using Eq.(7.3). If Eq.(7.3) is correct, all the values of T_{iso} thus obtained should be the same. However, the experimental values fluctuate over a large range of T_{iso} values, including negative numbers. These fluctuations arise from sequential decays and can be minimized by selecting double ratios with large binding energy differences ($B > 10$ MeV). However, such requirements select mainly isotope pairs that involve proton rich isotopes such as ^{3}He or ^{11}C which are not well bound. Thus instead of having many independent thermometers, there are in general two classes of isotopes thermometers, those involving the (^{3}He, ^{4}He) pair and those using (^{11}C, ^{12}C) pair. The fact that ^{3}He and to a lesser extent ^{11}C have been found to exhibit anomalous energy spectra may invalidate the simple relationship of Eq.(7.3).

The difference in shape of the energy spectra between ^{3}He and ^{4}He means that the isotope temperature depends on experimental energy thresholds. It has been shown that the temperature depends strongly on the energy gates used [64–67]. This dependence has been exploited to examine the evaporative cooling of the Xe on Cu collisions at E/A=30 MeV [65]. Since energy thresholds are often employed to minimize the contributions of the pre-equilibrium emissions [66,67], this directly affects the temperature values measured.

D. Effect of Sequential decays

In recent years, many models have been developed to describe the emission of particles from the multifragmentation process successfully. However, to compare with experimental data, these models must take into account the effects of sequential decays. Inclusion of nuclear spectral information into the calculations to simulate the effects of secondary decay has not been fully successful because the task is not only computationally difficult, but it is hampered by the lack of complete information about the resonances in many nuclei. Fig.9 shows the effect of sequential feedings on the temperature determination using two assumptions about the unstable states [68]. The horizontal axis is the emission temperature used in the statistical calculations [60] while the vertical axis is the apparent temperatures obtained using different classes of thermometers. In the left panel, sequential decay calculations including only known bound states and resonances are shown for T_{iso}(He-Li) and $T_{\Delta E}$(^{4}He), denoted by the solid and dashed lines respectively. The apparent isotope temperatures increase monotonically with the input temperature. With inclusion of continuum states (right panel), both temperatures flatten out at an asymptotic value of about 6 MeV. Thus, inclusion of sequential decay contributions from the continuum enhances decays to low-lying states and renders temperatures involving alpha particles insensitive to the emission temperature at high excitation energy. For comparison, the calculated excited state temperature of ^{5}Li (dot-dashed line) is plotted in the right panel: $T_{\Delta E}$(^{5}Li) continues to increase monotonically beyond 6 MeV emission temperature. The rate of increase becomes much less only after 9 MeV temperature.

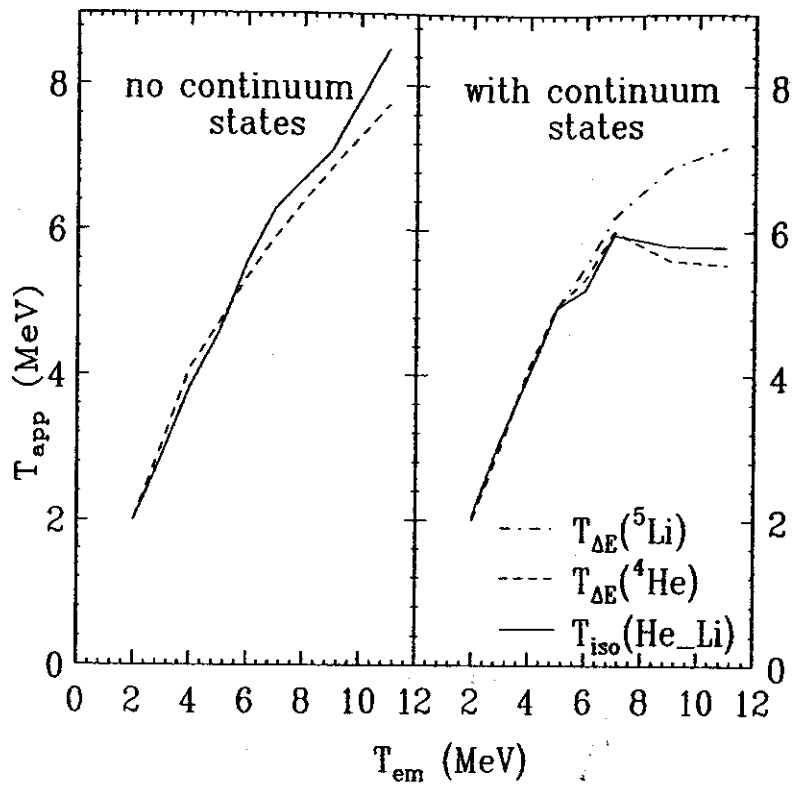

Fig. 9: Effect of sequential feedings on the temperatures determination using two assumptions on the unstable states [68]. In the left panel, sequential decay calculations including only known bound states and resonances are shown for T_{iso}(He-Li) and $T_{\Delta E}(^4He)$, denoted by the solid and dashed lines repectively. With inclusion of continuum states (right panel), both temperatures flatten out at an asymptotic value of about 6 MeV while the calculated excited state temperature of ^5Li (dot-dashed line) continues to increase monotonically until 9 MeV before flattening out [68].

Of course, the dependence of the apparent temperature on the emission temperature is model dependent. When the sequential decay effect is large such as at high temperature, reaction models with accurate description of the sequential decay processes are needed to relate the measured temperature to the emission temperature. Efforts have been made to include structural information to describe secondary decays. However, even with the best code available, the disagreement between measured and predicted isotope yields could be a factor of 10 or more especially for the neutron rich or proton-rich isotopes [69].

E. Cross-comparisons between thermometers

Cross-comparisons between different thermometers exist. In the case of kinetic temperature measurement, the slope of the energy spectra measured at backward angles and at low incident energy give reliable temperature information for systems with low excitation energy. Under these conditions, the collective flow effect and pre-equilibrium contributions are minimized. At higher energy, the kinetic temperatures are not reliable but one can cross-compare the isotope ratio and excited state temperatures [64,70–73]. Careful measurements of these

temperatures in various systems suggest that below E/A=35 MeV, there are good agreements between $T_{\Delta E}$ and T_{iso} [70]. However, the disagreement increases with incident energy [71,73] as shown in Fig.10. For the system of Kr+Nb, temperatures obtained from excited state populations and isotope yields have been measured as a function of the incident energy [73]. The open symbols represent the temperatures extracted from the excited state populations of ^{5}Li, ^{4}He and ^{8}Be respectively. Within experimental uncertainties, they are the same. The consistencies of the experimental results from different nuclei render credence to this thermometer. The closed symbols represent temperatures extracted from isotope yield ratios; T_{iso}(HeLi), (closed squares) rely on the double ratio [Y(^{6}Li)/Y(^{7}Li)] /[Y(^{3}He)/Y(^{4}He)] while T_{iso}(C-Li), (closed circles) use the double ratio [Y(^{6}Li)/Y(^{7}Li)] /[Y(^{11}C)/Y(^{12}C)]. Values for T_{iso}(C-Li) vary little with incident energy, similar to the trends exhibited by the excited states temperatures of ^{5}Li, ^{4}He, and ^{8}Be. In contrast, values of T_{iso}(He-Li) (closed squares) increase monotonically with incident or excitation energy. Similar discrepancies between $T_{\Delta E}$ and T_{iso} have been observed in Au + Au central collision from E/A=50 to 200 MeV [71], Ar+Sc reaction from E/A=50 to 150 MeV [75] and in Ar+Ni system [72] at E/A=95 MeV.

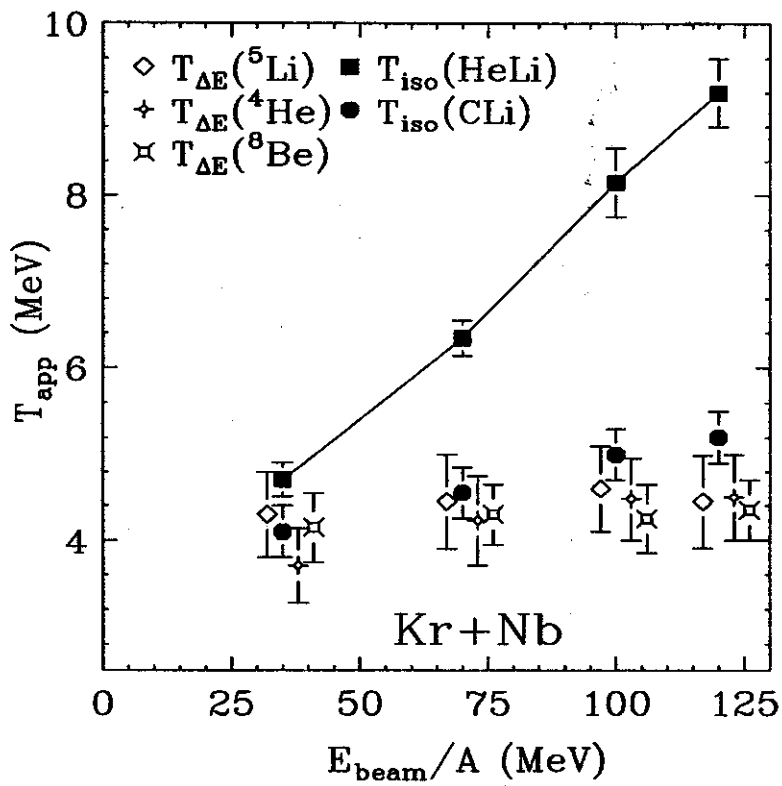

Fig. 10: Excitation function of different thermometers for the system Kr+Nb. The solid symbols are isotope ratio temperatures while the open symbols are temperatures extracted from excited states populations [73].

Independent of models describing sequential decays, thermometers using alpha particles (e.g. $T_{\Delta E}$(^{4}He),T_{iso}(He-Li)) should be affected by sequential decays in the same manner and should give the same experimental temperature. However, current data [60,71,72] show

that there are substantial differences between these two thermometers when the excitation energy or incident energy increases. This may indicate that different reaction mechanisms may be involved in the production of primary ^{3}He and ^{4}He particles. In such case, isotope yield temperatures constructed from Eq.(7.3) are problematic.

F. Summary of temperature measurements

Fig.11 shows an overall picture provided by the present data using different thermometers. The kinetic temperatures extracted from fitting the charged particle energy spectra with an intermediate rapidity source exhibit a smooth trend over a wide range of incident energies from a few MeV to nearly 1GeV per nucleons [74]. The open diamond points shown in Fig.11 are the proton kinetic temperatures extracted from [74] over a narrow range of incident energies for comparison purposes. The dashed lines are drawn to guide the eye. The temperature values depend slightly on the particle types. However, the other light charged particles, d and t, exhibit similar trends, namely, the kinetic energy temperature increases rapidly with the incident energy. A collection of the $T_{\Delta E}(^5\mathrm{Li})$ over a range of incident energies from 30 to 200 AMeV are plotted as solid points in Fig.11 [59,71,73]. Contrary to the kinetic temperature, there is only a slight increase from 3 to 5.5 MeV, in the excited state temperature as a function of the incident energy spanning over one order of magnitude. The open circles in Fig.11 represent the most commonly used isotope ratio temperature, T_{iso}(He-Li), [71,73,75] as a function of incident energy from 35 to 200 AMeV. The increase from 4 to 10 MeV as a function of incident energy is much less than T_{kin} but the increase is larger than the nearly constant value of $T_{\Delta E}(^5\mathrm{Li})$. T_{iso}(C-Li) are plotted as open diamonds in Fig.11. This latter isotope thermometer does not agree with T_{iso}(He-Li). Instead, T_{iso}(C-Li) remain relatively constant over the incident energy studied. They behave more like the excited state temperature.

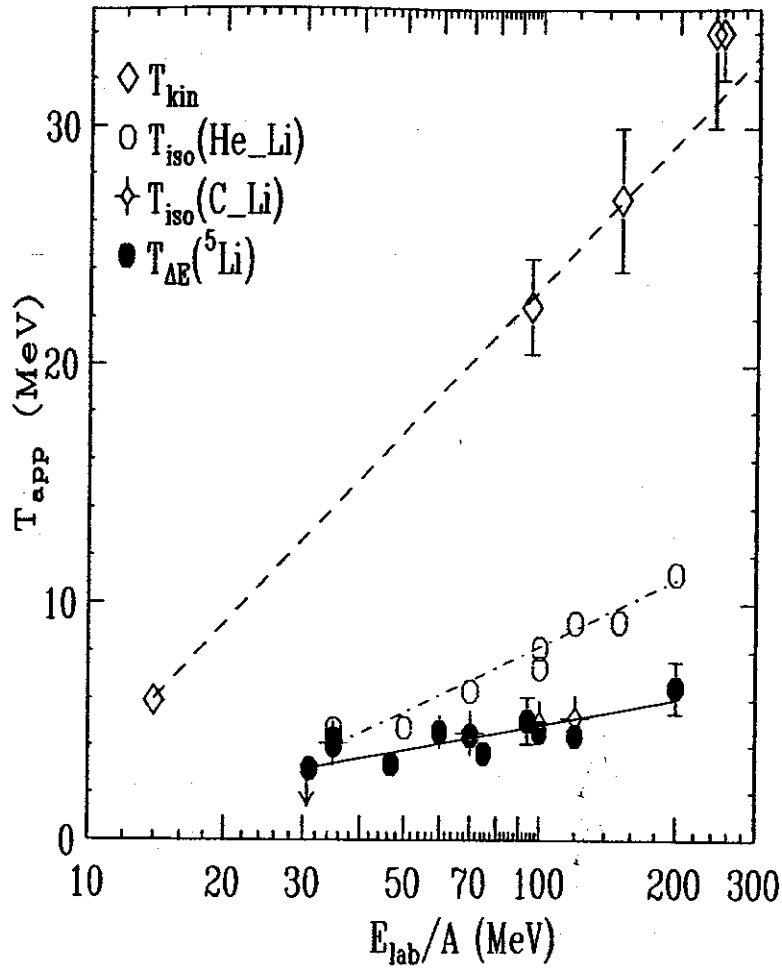

Fig. 11: Excitation function of proton kinetic temperature, (open diamonds with dashed lines drawn through the data), excited state temperature of ^{5}Li (solid circles and solid line), isotope ratio temperature of ^{3,4}He and ^{6,7}Li (open circles with dot-dashed lines) [76]

Experimentally, temperatures extracted from excited states or yield ratios involving carbon isotopes are around 4-5 MeV [77,59,73,69,63]. Around 4 MeV emission temperatures, the secondary decay effects are small and can be corrected with current models incorporating sequential decays. The near constant temperature may signal enhanced specific heat. However, if the low temperature of 4 MeV is caused by the limiting temperature due to sequential decays, it becomes difficult to deduce the freeze-out temperature from the measured quantities.

VIII. EXCITATION ENERGY DETERMINATION

In nuclear physics experiments, the collision conditions are reconstructed from the particles detected. Even if all the emitted particles can be measured experimentally, it is still difficult to disentangle the contributions from various emitting sources arising from the spectator and participant zones. Before multifragmentation occurs, the hot systems first deexcite by emitting neutrons and light charged particles (including very light IMF's). These

particles are normally emitted in the forward directions and in a very short time scale (<30 fm/c) before equilibrium is established. It is important that these pre-equilibrium particles are not included in the determination of excitation energy characterizing the fragmenting source.

Experimentally the contamination of the observables used in characterizing the emitting source is very difficult to assess without the use of model assumptions. Cascade and transport calculations can be used to estimate the number of particles emitted and the energy lost in the "prompt" or early stage of the reaction. Such calculations may suggest some optimum ways of estimating the number such as imposing energy thresholds on the data to minimize the "pre-equilibrium" contributions [48,78]. However, the prompt contributions cannot be completely eliminated from the data using the energy threshold gates. This increases the uncertainties and fluctuations in the excitation energy determined. The model calculations may also indicate the size, mass, N/Z ratio and energy of the residues which undergo "multifragmentation". Assume we can detect and identify all the particles emitted from this excited source, conservation of energy suggests that

$$E^* = \sum E_i + \sum E_n + \sum E_\gamma + Q \tag{8.1}$$

Where E^* is the excitation energy, E_i is the kinetic energy of the charged particles, E_n is the energy of the neutrons, E_γ is the energy of the gamma rays emitted during the de-excitation and Q is the mass difference between the parent nucleus and all the emitted particles. Gamma energies are relatively small and contribute little to the total excitation energy compared to the other terms.

In reality, most experimental apparatus does not have a complete 4π coverage. Furthermore, thresholds in energy and geometry exist in the detection arrays. Thus there are uncertainties in determining the terms $\sum E_i$ and Q. More importantly, neutrons are often not measured. Neutrons do not interact with matter as much as the charged particles so they are more difficult to detect. Very often, $\sum E_n$ is estimated using the average number of neutrons emitted and the mean neutron energy, $\sum E_n = N_n < E_n >$ [48,10,78]. Conservation of particles imposes some constraints on the value of neutron multiplicity N_n. As the neutron data is difficult to obtain, the mean neutron energy $< E_n >$ values are usually adopted from other experiments or assumed to be the same as the proton mean energy. Therefore in general, $\sum E_n$ poses the largest uncertainty to Eq.(8.1) and determination of excitation energy of the fragmenting system becomes quite a difficult task.

Recently, intense effort has been placed in extracting the excitation energy of heavy nuclei induced by high-energy hadron beams such as protons, pions and anti-protons at high energy [79]. In these reactions, the collective excitation and existence of multiple sources are minimal. Even with such "simplified" systems, it is difficult to extract precise excitation energy without the use of model assumptions. For heavy ion reactions, the task is much more daunting. In addition, all collective motions strongly affect the signals of the phase-transition and must be understood before exact values of the excitation energy can be assigned. With so many uncertainties associated with extracting the excitation energy, any experimental observables that utilize the fluctuations of excitation energy such as measuring the heat capacities are subjected to the same problems [80]. The results must be viewed cautiously. While more work is needed to determine the excitation energy accurately, one consensus is that increasing incident energy corresponds to increasing excitation energy.

It is quite common to extract the excitation enegy using projectile fragmentation. Assuming that the projectile is only modestly excited, only one source, the projectile-like residue, exists. Then the excitation energy of the projectile-like residue should be inversely proportional to impact parameter. Thus it has been argued that Z_{bound}, rather directly, reflects the energy transfer to the excited spectator system [10]. Larger energy transfers, then, correspond to smaller value of Z_{bound} and vice versa. However, geometrical arguments suggest that the source size also varies with impact parameter [81]. Furthermore, the energy spectra of light charged particles are inconsistent with one source but require multiple sources to fit the spectra [73]. It is thus incorrect to assume that there are no contributions from pre-equilibrium emissions. As discussed previously, collective flow also plays a role in projectile fragmentation. Besides, all the uncertainties associated with Eq.(8.1) as described above apply to these reactions.

Currently determination of the excitation energy presents the biggest challenge to the experimenters. With care and the increasing availability of large neutron detection devices, the excitation energy measurements will be improved in the coming years. A firm grip of this parameter is very important in our understanding of the liquid-gas phase-transition.

IX. SIGNALS FOR LIQUID-GAS PHASE TRANSITIONS

Over the years, many experimental observables involving IMF have been used to study the nuclear liquid-gas phase transition. Discussions of all the proposed experimental signatures will require too much time and space. Instead, we will focus our discussions on four experimental signatures, which have attracted most attention in the past years.

A. Rise and Fall of IMF

Copious emission of intermediate mass fragments is one predicted consequence of the liquid-gas phase transition of nuclear matter, both by statistical models and transport models. At low excitation energy, few fragments are "evaporated" from the liquid while at very high excitation energy, the liquid "vaporizes" to produce a nucleon gas. The "rise and fall" of IMF multiplicities has been observed in both central and peripheral collisions. For central collisions, maximum fragment productions occur around incident energy of 100A MeV as shown in the left panel of Fig. 12 for the Kr+Au reaction [82]. At incident energy above 400A MeV, production of IMF shifts from central to more peripheral collisions [83,84]. The right panel of Fig.12 shows the impact parameter dependence (obtained by measuring Z_{bound} for the fragmentation of Au projectiles at incident energy from 400 MeV to 1 GeV [83]. In both panels of Fig.12, fragment multiplicities increase to a maximum with increasing excitation energy. The fragment production then declines and "vaporizes" completely into nucleons and light particles.

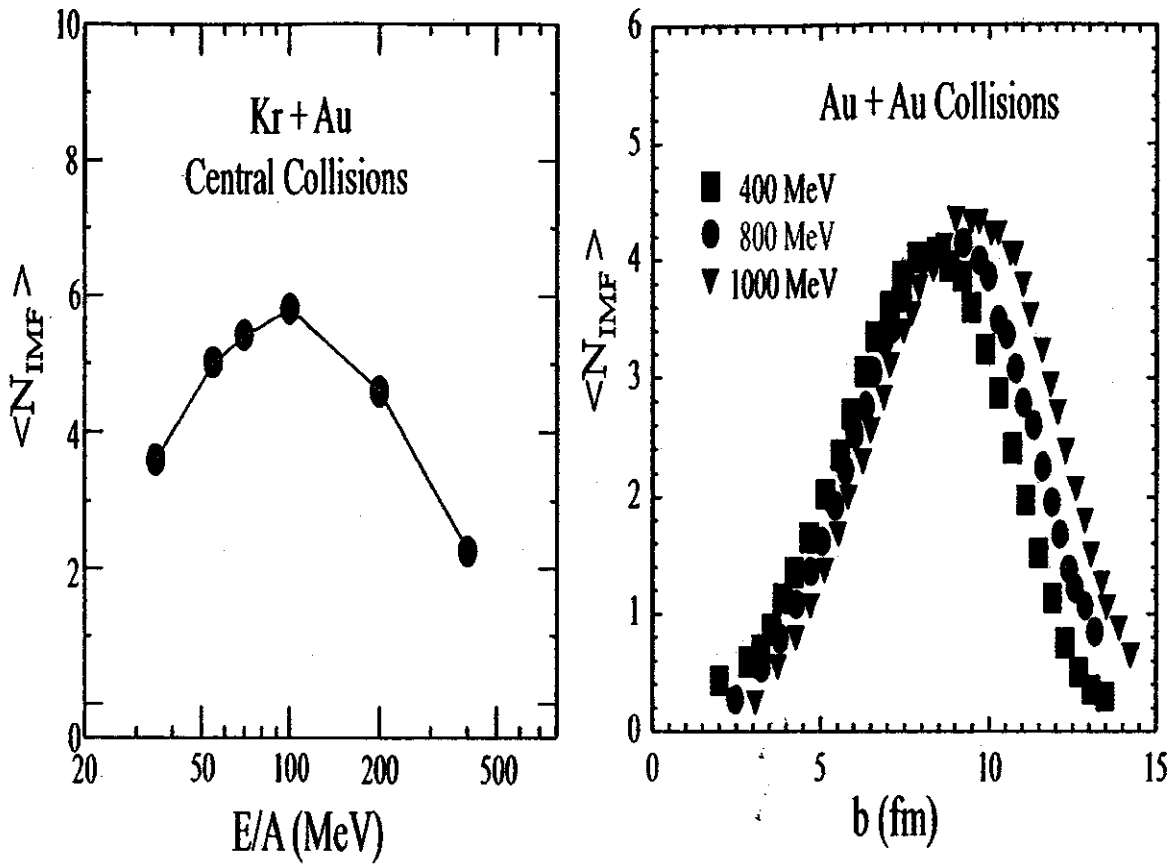

Fig. 12: Rise and fall of IMF multiplicity as a function of incident energy for the central collisions of Kr + Au (left panel) [82] and as a function of impact parameters for the projectile multifragmentation of Au+Au reactions (right panel) [83].

B. Critical Exponents

The observation by the Purdue group [17] that the yields of the fragments produced in p+Xe and p+Kr obeyed a power law $Y(A_f) \propto A_f^{-\tau}$ led to a conjecture that the fragmenting target was near the critical point of liquid-gas phase transition. The origin of this conjecture is the Fisher model [85] which predicts that at the critical point the yields of droplets will be given by a power law. The power law has since then been established very firmly in collisions between heavy ions [83] with the value of the exponent τ being close to 2. But the power law is no longer taken as the 'proof' of criticality. There are many systems that exhibit this sort of power law: mass distributions of asteroids in the solar system, debris from the crushing of basalt pellets [86] and the fragmentation of frozen potatoes [87]. In fact, the lattice gas model which has been used a great deal for calculations of phase transitions and multifragmentation in nuclei [88,89] gives a power law at the critical point, on the coexistence curve (that is a first order phase transition provided the freeze-out density is less than the critical density) and also along a line in the $T - \rho$ plane away from the coexistence curve. Nonetheless, the occurrence of a power law is an experimental fact and it is therefore desirable that models which aim to describe multifragmentation produce a power law, phase transition or not.

Even if we expect to see a phase transition in nuclear collisions it is unlikely that the system dissociates at the critical point. Much of the literature in intermediate energy heavy-ion collisions assumes that when one is seeing a phase transition one is actually seeing critical phenomena [90,91]. To reach the critical point one has to hit the right temperature and the right density. While one may be able to hit the right temperature by varying the beam energy, one has no control over the freeze-out density. Thus it is unlikely that the dissociation takes place at the critical point. We think that this strong emphasis on critical phenomenon rather than first order phase transition in nuclear multifragmentation came about for several reasons. Firstly, the experimentally observed power law was interpreted in terms of critical phenomena. Secondly, a bond percolation model [92–96] was among the first to be applied to multifragmentation in nuclear collisions. This model has only a continuous phase transition. The bond percolation model can be demonstrated to be a special case of a lattice gas model [97] which is more versatile and has both first order phase transition and critical phenomena.

An excellent review of the early history of this topic exists [98]. This covered the period to the end of 1984. More recently, the study of the liquid-gas phase transition in nuclear matter focuses more on measuring the thermodynamical properties, such as the temperature and densities, of the disassembling system.

C. Nuclear Caloric Curve

Experimentally, production of particles in multifragmentation appears to be dominated by their phase space [42,54,99]. Thus, one should be able to measure temperature and densities, basic quantities in statistical physics. If the liquid-gas phase transition is of first order, one would expect to see enhanced specific heat dE^*/dT corresponding to a plateau region in the caloric curve defined as temperature, T vs. heat or excitation energy E^*/A. Aside from the experimental difficulties associated with measuring both quantities as discussed in sections 7 and 8, the simple caloric curve of temperature vs. excitation energy with a plateau in the temperature assumes that the pressure is constant [100]. There is no experimental evidence that such a condition is met in nuclear collisions. Thus even without introducing the isospin degree of freedom, the caloric curves depend on three variables, pressure, volume and temperature. Such complicated, three-dimensional nuclear caloric curves have been recently calculated [101]. Different shapes of the caloric curves have been obtained depending on the conditions of the experiments and analysis. Therefore, one-dimensional caloric curves are useful only if the exact conditions can be determined or modeled. By themselves, these curves can be misleading and definitely do not constitute a signature for the liquid-gas phase transition even though the idea is very attractive.

One of the purposes of this review article is to examine the experimental efforts in extracting the liquid-gas phase transition signals. Since many caloric curves have been measured since 1995, we will discuss the experimentally obtained curves keeping the above "warnings" in mind.

If the incident energy is assumed to be related to the excitation energy, (this is particularly true for central collisions), then Fig.11, which is a plot of temperature versus incident energy from E/A=30 to 200 MeV, is one form of caloric curve. It shows that the trend depends highly on the specific thermometers chosen to measure the temperature; the kinetic

temperature increases rapidly (from 12 to 30 MeV); the excited states temperatures are nearly constant (from 3 to 7 MeV); the isotope temperatures involving He isotopes increase moderately (from 4 to 10 MeV) but isotope temperatures involving ^{11}C,^{12}C stay nearly constant at 4 MeV. Fig.11 sums up the most serious experimental problems we are faced with i.e. the discrepancies in the temperature measurements. However, this figure also shows that the excitation functions of the temperature measurement exhibit a smooth behavior within each class of thermometer. Moreover, the trends are consistent from experiment to experiment since the data shown in Fig.11 come from many different sources.

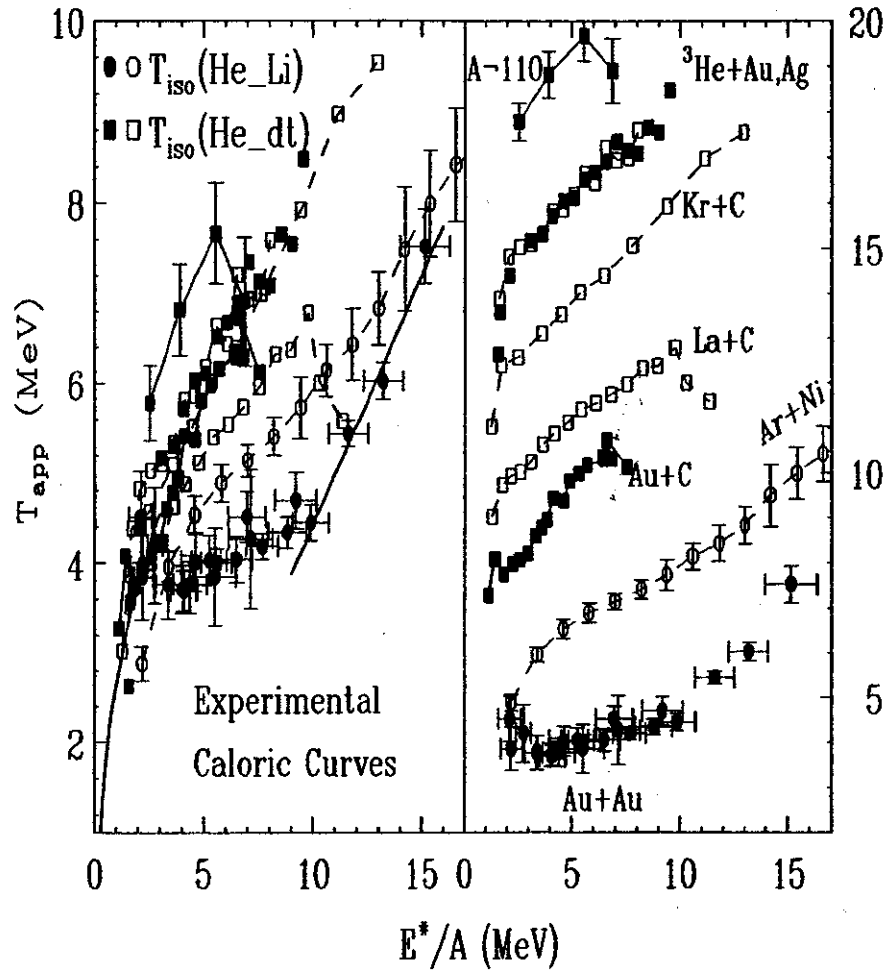

Fig. 13: Summary of caloric curves measured. The curves in the right panel have been offset by 2 MeV for each successive curve, starting with Ar+Ni.

The more traditional caloric curves which plott temperatures versus the extracted excitation energy are shown in Fig.13. In the left hand panel, all the curves are plotted on the same scale. The temperatures obtained have been extracted using the isotope yield ratios; T_{iso}(He-Li) are denoted by circles and T_{iso}(He-dt) are represented by the squares. To avoid confusions, all the temperatures plotted are the experimental apparent temperatures since sequential decay corrections are highly model dependent. Sequential decays account for part of the differences between T_{iso}(He-Li) and T_{iso}(He-dt) and there are empirical cor-

rection factors to reduce such differences. However, in this plot, the differences between the curves constructed with T_{iso}(He-Li) or T_{iso}(He-dt) are much larger than the correction factors. Thus, to keep the discussion simple, only the reported raw data are shown.

In order to view each successive curve better, they are re-plotted in the right panel with a scale compressed by a factor of 2. Each curve is offset from from its predecessor by 2 MeV and the corresponding reactions are labelled close to the curves. The most interesting curve is the one labeled "Au+Au" plotted at the bottom of both the right and left panels. It was obtained from the spectator decays of the Au+Au reaction at E/A=600 MeV [10]. T_{iso}(He-Li), remains relatively constant as a function of deduced excitation energy, E*/A, between 3 and 10 MeV but increases rapidly at E*/A greater than 10 MeV. The resemblance to the first order phase transition of liquid raises a lot of excitement in the field. It also resembles the prediction from the statistical model [102].

Unlike the predicted caloric curves from realistic models which will be discussed in more details in Section XII or the temperature excitation functions of Figure 11, the experimental caloric curves depend strongly on the reaction systems and analysis. (Due to the effect of sequential decay, caloric curves determined from the experimentally extracted isotope yields may not resemble the curves of the deduced primary fragments [67].) On the other hand, if one ignores the highest excitation data point in the Au+Au system, all caloric curves exhibit a smooth increase of temperature with excitation energy. This trend is very similar to the increase of T_{iso}(He-Li) as a function of incident energy as shown in fig.11. However in that case, the excitation function of the T_{iso}(He-Li) is nearly independent of reaction systems, Au+Au, Kr+Nb and Ar+Sc reactions, measured by different experimental groups. The differences in the curves shown in Figure 13 again point to the uncertainties associated with the experimental procedures in extracting temperature and excitation energy.

All the caloric curves measured so far suffer from the same uncertainties in determining the excitation energy. Some data may have better handle on the excitation energy because of better detector coverage or simpler reaction mechanisms. For example, the caloric curves obtained from the projectile fragmentation of Au, La and Kr on C, [67] have been extracted with a time-projection chamber (EOS-TPC) where a complete reconstruction of the projectile charge can be accomplished. The curves obtained from Au+C and Kr+C overlap very nicely with each other even though the La+C system shows lower temperatures measured. (The experimenters of Ref. [67] claim that the discrepancies observed in the temperatures (15%) are within the experimental uncertainties.) It is also encouraging to see that these two curves overlap with the ^{3}He+Au and ^{3}He+Ag data which used similar procedures in determining the temperatures and excitation energy [103].

Many of the extracted caloric curves do not agree with each other. Part of the differences can be attributed to the energy thresholds applied to extract the isotope yields. The high energy thresholds used in the A$\approx$100 systems to isolate the prompt component [104] probably account for the highest temperatures obtained in all the curves. For the Au+C, La+C, Kr+C, [67] ^{3}He+Au, and ^{3}He+Ag [103] systems, assumptions have been made regarding the pre-equilibrium contributions and the missing neutrons. Energy thresholds are used to eliminate pre-equilibrium emissions. This might account for the relatively high temperatures measured as compared to the temperatures extracted from Au+Au reaction. In the latter case, the pre-equilibrium contributions were minimized using other methods and attempts were made to extrapolate yields to zero energy thresholds.

In the past year, some of the caloric curves have been revised [67] and others including the original "caloric curve" data are being reanalyzed [10,105]. With more attention paid to the experimental problems associated with determining these curves, some of the discrepancies might be resolved in the near future. Future studies might extract other underlining physics from these data. Without further understanding of the reaction dynamics and experimental limitations, one should be extremely cautious in interpreting these curves as experimental signatures for the liquid-gas phase transitions of nuclear matter.

D. Isospin Fractionation

Since nuclei are composed of neutrons and protons, isospin effects may be very important for the nuclear liquid-gas phase transition [106]. As the asymmetry between neutron and proton densities becomes a local property in the system, calculations predict neutrons and protons to be inhomogenously distributed within the system resulting in a relatively neutron-rich gas and relatively neutron-poor liquid [107–109]. The critical temperature may also be reduced with increasing neutron excess reflecting the fact that a pure neutron liquid probably does not exist [107]. While, recent calculations suggest that the rather narrow range of isospin values available in the laboratory might not allow us to observe the decrease in critical temperature [110], efforts are underway to study the fractionation of the isospin in the co-existence region. As the isospin effects are not large, the influence of sequential decays becomes important and may obscure the isospin fractionation effect one wishes to study. To minimize such problems, isobar pairs, such as (t,^{3}He), which have the same number of internal excited states have been used. Some indications for isospin fractionation are provided by the sensitivity of Y(t)/Y(^{3}He) distributions to the overall N/Z ratio of the system [33]. The ratios of Y(t)/Y(^{3}He) also have been observed to decrease with incident energies, in qualitative agreement with the predictions from the isospin dependent lattice gas model [109,111,112]. Light isobars such as (t,^{3}He) pair may suffer from contamination of pre-equilibrium processes. Attempts have been made to use additional mirror isobar pairs such as (^{7}Li, ^{7}Be) and (^{11}B, ^{11}C) [30].

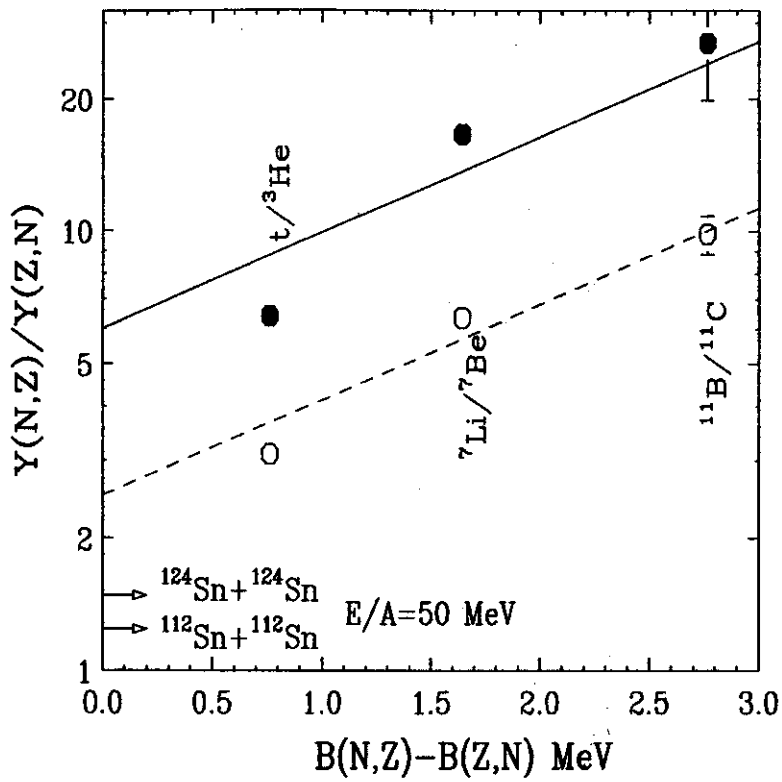

Fig. 14: Isobar ratios for three mirror nuclei obtained from the ^{112}Sn+^{112}Sn (open circles) and ^{124}Sn+^{124}Sn (solid points) reactions [30]. The lines are drawn to guide the eye.

Fig.14 shows the isobaric yield ratios of 3 pairs of mirror nuclei as a function of the binding energy difference, ΔB for two reactions, ^{112}Sn+^{112}Sn (open points) and ^{124}Sn+^{124}Sn (solid points) at E/A=50 MeV. If the sequential decay and the Coulomb effects are small, the dependence of the isobaric yield ratios on the binding energy difference should be exponential, i.e. of the form $(\rho_n/\rho_p)\exp(\Delta B/T)$ where ρ_n and ρ_p are the neutron and proton densities. The experimental data fluctuate around such a relationship. Extrapolation to $\Delta B = 0$ using best fit lines (dashed and solid lines) allows one to obtain values for ρ_n/ρ_p of 2.5 for the ^{112}Sn+^{112}Sn system (top line) and 5.5 for the ^{124}Sn+^{124}Sn system (bottom line). Both of these numbers are larger than the initial N/Z values of the two system, 1.24 and 1.48 for ^{112}Sn+^{112}Sn and ^{124}Sn+^{124}Sn, respectively. The change in the N/Z values of the two systems is about 20%. However the changes between any of the mirror nuclei ratios are of the order of 200%, much larger than what one expects if the extracted neutrons introduced into the neutron rich systems are homogenously distributed. This observation suggests that the free neutron density needed to determine the light particle yields emitted from multifragmentation is much enhanced in the neutron rich system.

To bypass the sequential decay problems completely and to avoid using only selected ratios, an observable employing ratios of all measured isotope yields is used. This method relies on extracting the relative neutron and proton density from two similar reactions, which differ mainly in isospin. Adopting the approximation of a dilute gas in the Grand-Canonical Ensemble limit with thermal and chemical equilibrium, the production of isotopes with neutron number N and proton number Z are governed by the nucleon densities, ρ_n, ρ_p, the

temperature T plus the individual binding energies of the various isotopes B(N,Z).

$$Y(N,Z) = F(N,Z,T)\rho_n.\rho_p.\exp(B(N,Z)/T \tag{9.1}$$

The factor $F(N,Z,T)$ includes information about the secondary decay from both particle stable and particle unstable states to the final ground state yields as well as the volume terms. (Some readers may notice the similarity of Eq.(9.1) to the Saha equation used to describe the nucleation of a neutron and proton gas in astrophysics. In that case the prefactor F(N,Z,T) is dominated by the entropy term.) If one constructs the ratio of $Y(N,Z)$ from two different related reactions, the observable called the relative isotope ratio, $R_{21}(N,Z)$ has a simple dependence on the relative neutron density and proton density of the free nucleon gas.

$$R_{12}(N,Z) = \frac{Y_2(N,Z)}{Y_1(N,Z)} \approx (\frac{\rho_{n,2}}{\rho_{n,1}})^N(\frac{\rho_{p,2}}{\rho_{p,1}})^Z = \hat{\rho_n}^N\hat{\rho_p}^Z \tag{9.2}$$

In the study of the central collisions of four Sn systems at incident energy of 50 MeV per nucleon [30], the relative neutron and proton densities have been measured for the ^{112}Sn+^{124}Sn (N/Z=1.36), ^{124}Sn+^{112}Sn (N/Z=1.36), ^{124}Sn+^{124}Sn (N/Z=1.48)with respect to the ^{112}Sn+^{112}Sn (N/Z=1.24) system. More than 20 isotope ratios are measured and they follow the dependence of Eq.(9.2) very well [30,113].

The extracted $\hat{\rho_n}$ and $\hat{\rho_p}$ ratios are shown in Fig.15; $\hat{\rho_n}$ increases while $\hat{\rho_p}$ decreases with the N/Z ratio of the total system. The increase of $\hat{\rho_n}$ is consistent with neutron enrichment in the gas phase while the decrease of $\hat{\rho_p}$ suggests proton depletion, a consequence of n-enrichment in the nucleon gas. The experimental trend (data points with the solid line drawn to guide the eye) is much stronger than the trend expected if neutrons and protons were homogeneously mixed (dashed lines) in the breakup configuration. Adopting an equilibrium breakup model, results of Figs. 14 and 15 are consistent with isospin fractionation, a signal predicted in the liquid-gas phase transition. However, as with other signatures for phase transition observed so far, since the isospin fractionation is governed by the symmetry energy of the neutron and proton, "isospin fractionation" is a more general characteristic of heavy-ion reaction than the liquid-gas phase phenomenon. In fact, dynamical models also give predictions of isospin amplication, in qualitative agreement with the data [114].

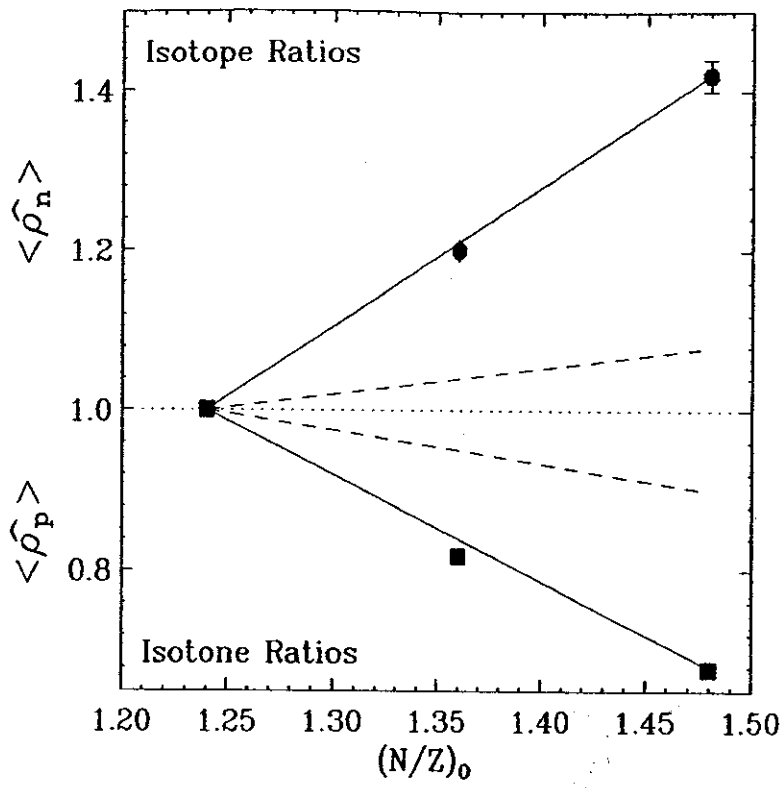

Fig. 15: The mean relative free neutron and free proton density as a function of $(N/Z)_O$. The dashed lines are the expected n-enrichment and p-depletion with the increase of isospin of the initial systems. The solid lines are drawn to guide the eye [30].

X. A CLASS OF STATISTICAL MODELS

A class of statistical models has been very successful in explaining multifragmentation processes in heavy-ion collisions. These models assume the following scenario. One defines a freeze-out volume. At this volume an equilibrium statistical machanics calculation is done. However, these statistical calculations do not start from a fundamental two-body interaction or even a simplified schematic two-body interaction. Instead the inputs are the properties of the composites (which appear as bound objects because of the fundamental two-body interaction); their binding energies and the excited states. Their populations are solely dictated by phase-space. This is very similar to chemical equilibrium between perfect gases as, for example, discussed in [3]. The only interaction between composites is that they can not overlap with each other in the configuration space. Coulomb interaction between composites can be taken into account in different stages of approximation. These models have the virtue that they can be used to calculate data for many experiments whether these experiments relate to phase transition or not. The Copenhagen model, a statistical multifragmentation model abbreviated SMM (also referred to as SMFM), has become, *de facto*, the "shell-model" code for intermediate energy heavy ion data. An excellent review of this model exists [102]. The Berlin Model, a microcanonical multifragmentation model, usually abbreviated MMMC, has also been used to fit experimental data [115]. Some other references for microcanonical simulation of similar physics are [116,117]. While there have been tremendous improvements in techniques and details, the roots of such models for heavy-ion collisions go back more than 20 years [118].

With some simplifications, the model of composites within the freeze-out volume at a given temperature can be exactly solved. In order to distinguish this model from SMM and MMMC (which are much harder to implement) we will coin a name. We will call this the thermodynamic model. As phase transition aspects are easily studied in the model, we treat this in detail.

XI. A THERMODYNAMIC MODEL

If there are A identical particles of only one kind in an enclosure, the partition function of the system can be written as

$$Q_A = \frac{1}{A!}(\omega)^A \tag{11.1}$$

Here ω is a one-particle partition function of the particle. For a spinless particle this is $\omega = \frac{V}{h^3}(2\pi mT)^{3/2}$; m is the mass of the particle; V is the available volume within which each particle moves; $A!$ corrects for Gibb's paradox. One might argue that this is not a rigorous way of treating symmetry or antisymmetry of particles but a recent paper [119] demonstrates that for nuclear disassembly this correction is very adequate. If there is only one species, eq.(11.1) is trivially calculated.

If there are many species, the generalisation is

$$Q_A = \sum \Pi_i \frac{(\omega_i)^{n_i}}{n_i!} \tag{11.2}$$

Here ω_i is the partition function of a composite which has i nucleons. We are at the moment ignoring the distinction between a neutron and a proton and thus our composites are bound states of i nucleons. For a dimer, $i = 2$, for a trimer, $i = 3$ etc. In a more realistic version we will introduce the distinction between neutrons and protons but this model of one type of nucleon is highly illustrative, so we will continue with this for a while.

Eq.(11.2) is no longer trivial to calculate. The trouble is with the sum in the right hand side of eq.(11.2). The sum is restrictive. We need to consider only those partitions of the number A which satisfy $A = \sum i n_i$ This restriction is hard to implement in an actual calculation and already for A of the order of 100, the number of partitions which satisfies the sum is enormous. We can call a given allowed partition a channel. The probablity of the occurrence of a given channel $(n_1, n_2, n_3.....)$ is

$$P(\vec{n}) \equiv P(n_1, n_2, n_3.....)$$

$$P(\vec{n}) = \frac{1}{Q_A} \Pi \frac{(\omega_i)^{n_i}}{n_i!} \tag{11.3}$$

The average number of composite of i nucleons is easily seen from Eq.(11.3) to be

$$< n_i >= \omega_i \frac{Q_{A-i}}{Q_A} \tag{11.4}$$

Since $\sum i n_i = A$ one readily arrives at a recursion relation [120]

$$Q_A = \frac{1}{A} \sum_{k=1}^{k=A} k \omega_k Q_{A-k} \tag{11.5}$$

For one kind of particle, Q_A above is easily evaluated on a computer for A as large as 3000 in matter of seconds. Thus in this model we can explore the thermodynamic limits. It is this recursion relation that makes computation so easy in the model. In the realistic model with two kinds of particles which we will introduce later, systems as large as 400 particles are easily done. It is important to realise that millions of channels possible in the partitions (Eq.(11.3)) are exactly taken into account, although numerically. No Monte-Carlo sampling of the channels is required.

We now need an expression for ω_k which can mimic the nuclear physics situation. We take

$$\omega_k = \frac{V}{h^3} (2\pi m T)^{3/2} k^{3/2} \times q_k \tag{11.6}$$

where the first part arises from the centre of mass motion of the composite which has k nucleons and q_k is the internal partition function. For $k = 1, q_k = 1$ and for $k \geq 2$ it is taken to be

$$q_k = \exp[(W_0 k - \sigma(T) k^{2/3} + T^2 k/\epsilon_0)/T] \tag{11.7}$$

Here, as in [102], W_0=16 MeV is the volume energy term, $\sigma(T)$ is a temperature dependent surface tension term and the last term arises from summing over excited states of the composite in the Fermi-gas model. For high temperatures, this will overestimate the contribution of

the excited states and a modified expression is sometimes used to correct for this [116]. The explicit expression for $\sigma(T)$ used here is $\sigma(T) = \sigma_0[(T_c^2 - T^2)/(T_c^2 + T^2)]^{5/4}$ with σ_0= 18 MeV and T_c=18 MeV. The value of ϵ_0 is taken to be 16 MeV. The energy carried by one composite is given by $E_k = T^2 \partial ln\omega_k/\partial T = \frac{3}{2}T + k(-W_0 + T^2/\epsilon_0) + \sigma(T)k^{2/3} - T[\partial\sigma(T)/\partial T]k^{2/3}$. Of these, the first term comes from cm motion and the rest from q_k. In [121], the term $T[\partial\sigma(T)/\partial T]k^{2/3}$ was neglected. It is included here but makes little difference. In the nuclear case one might be tempted to interpret the V of Eq.(11.6) as simply the freeze-out volume but it is clearly less than that; V is the volume available to the particles for the centre of mass motion. In the Van der Waals spirit we take $V = V_{freeze} - V_{ex}$ where V_{ex} is taken here to be constant and equal to $V_0 = A/\rho_0$ [122]. The precise value of V_{ex} is inconsequential so long it is taken to be constant. Calculations employ V; the value of V_{ex} enters only if results are plotted against $\rho/\rho_0 = V_0/(V + V_{ex})$ where ρ is the freeze-out density. The energy of the system is $E = \sum < n_k > E_k$; the pressure is $p = T\partial lnQ_A/\partial V = T\frac{1}{V}\sum < n_i >$. These can be deduced from Eqs.(11.2) and (11.4).

The surface tension term is crucial for phase transition in this model. At a given temperature the free energy $F = E - TS$ has to be minimised. It costs in the energy term E to break up a system. A nucleus of A nucleons has less surface than the total surface of two nuclei each of $A/2$ nucleons (the volume energy term has no preference between the two alternatives). Therefore at low temperature one will see a large chunk. The $-TS$ term favours break up into smaller objects. The competition between these two effects leads to the following features seen in experiments. At low temperature (low beam energy) each event will have one large composite (the fission channel is not included in these models) and few small composites. This leads to the inclusive cross-section being U-shaped (Fig.16). (For illustration, starting from this figure and and upto and including Fig.20, all calulations employ V of Eq.(11.6) =1.5V_0). As the temperature increases, the peak on the large a side begins to decrease, finally disappearing entirely. When this happens, one has crossed from the coexistence zone to the gas phase. A graph of the yield $Y(a)$ against a is shown in Fig.16. At temperature 6.2 MeV one sees both a large residue and smaller clusters, at 6.7 MeV the large cluster just disappears and at 7.2 MeV one has only the gas phase.

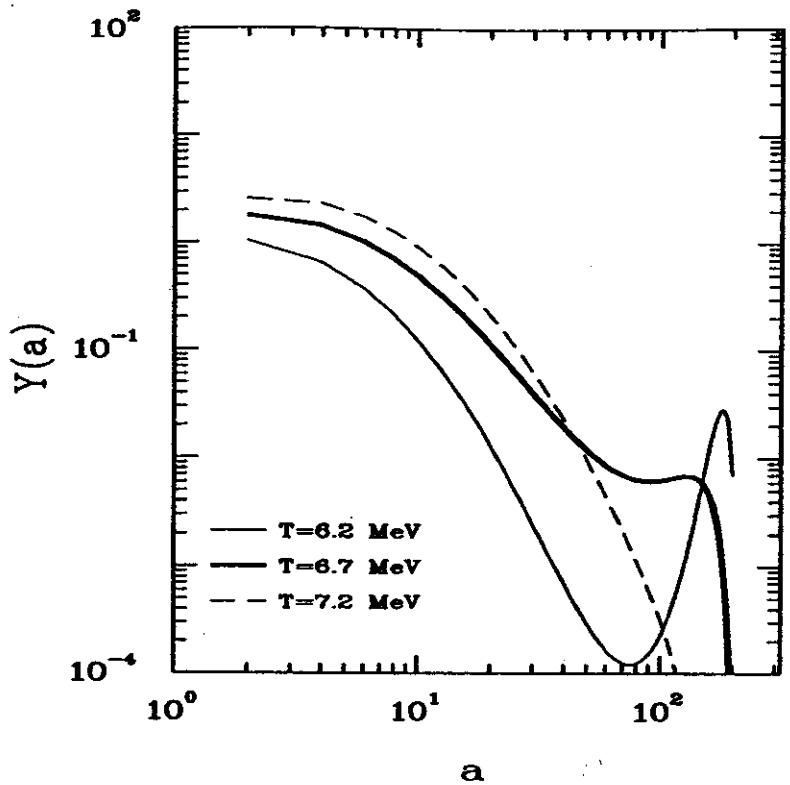

Fig.16. In a model of one kind of nucleon, the yield $Y(a)$ against a where the disintegrating system has 200 nucleons. At temperature 6.2 MeV one has coexistence: on the average, there is a large blob and also lighter mass composites. At 6.7 MeV, the maximum in the yield $Y(a)$ on the high mass side just disappears.. This is also the temperature at which the specific heat C_v per particle maximises (see Fig.17). We call this the boiling temperature. At higher temperature, the yield $Y(a)$ falls monotonically.

It is instructive to plot for the same nucleus the specific heat per nucleon labelled by C_v, the total multiplicity and N_{IMF}, the number of intermediate mass fragments as a function of temperature (Fig.17). One sees the specific heat maximising at the same temperature as the one at which, in Fig.16, the peak in the high a side of the yield function $Y(a)$ just disappears. One should remember that fragments produced in this model appear at non-zero temperature. They will further decay by sequential emissions. Thus the total multiplicity plotted here is lower than actual value to be expected finally. After the sequential decays, the yields of very light elements such as monomers, dimers etc. will increase substantially as the heavy composites decay by emitting these. In N_{IMF} in Fig.17 we have included a=6 to 40. With sequential decays included N_{IMF} will go down from the values shown in Fig.17.

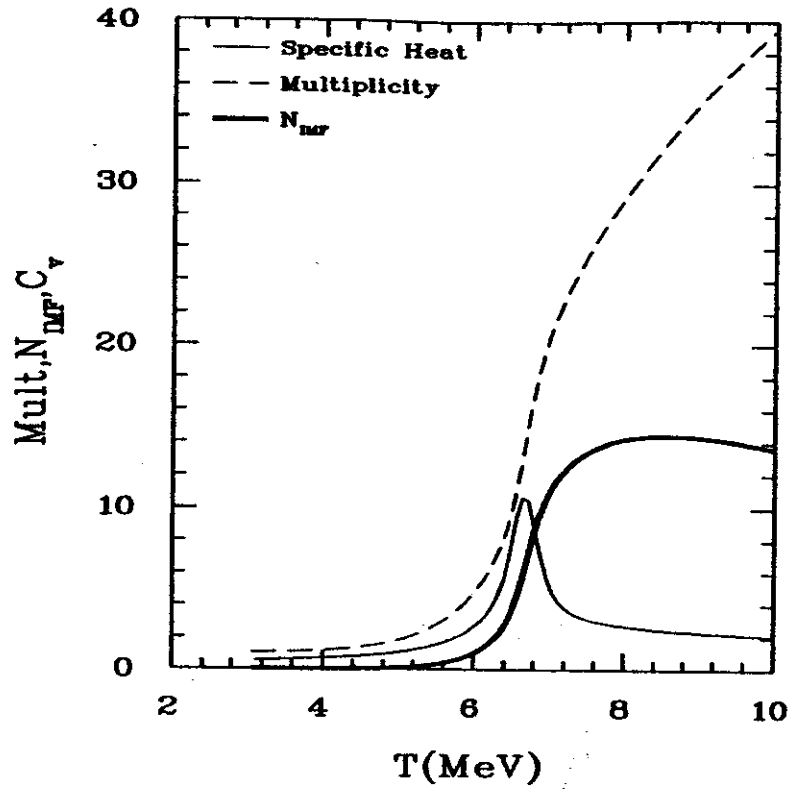

Fig.17. For the same model of 200 nucleons of one kind, the total multiplicity, N_{IMF} (the number of intermediate mass fragments defined here as having a between 6 and 40) and the specific heat C_v per particle as a function of temperature. Note that the maximum of the specific heat coincides with the quick rise in N_{IMF} and the disappearence of the maximum in the yield $Y(a)$ on the high a side.

Keeping these reservations in mind we see in Fig.17 that the sudden increase of the multiplicity and N_{IMF} imply coexistence. At higher temperature, the system is in the gas phase. The cross-section for a large residue is very small (Fig.16). In order to understand the nature of the phase transition we now go to much larger systems so that one can feel confident about extrapolation to the thermodynamic limit. With this in mind we have plotted in Fig.18., for a system of 1400 and 2800 particles, the free energy per particle as a function of temperature (The free energy is simply $-TlnQ_A$). A brake appears to develop in the first derivative of F/A which signifies first order phase transition.

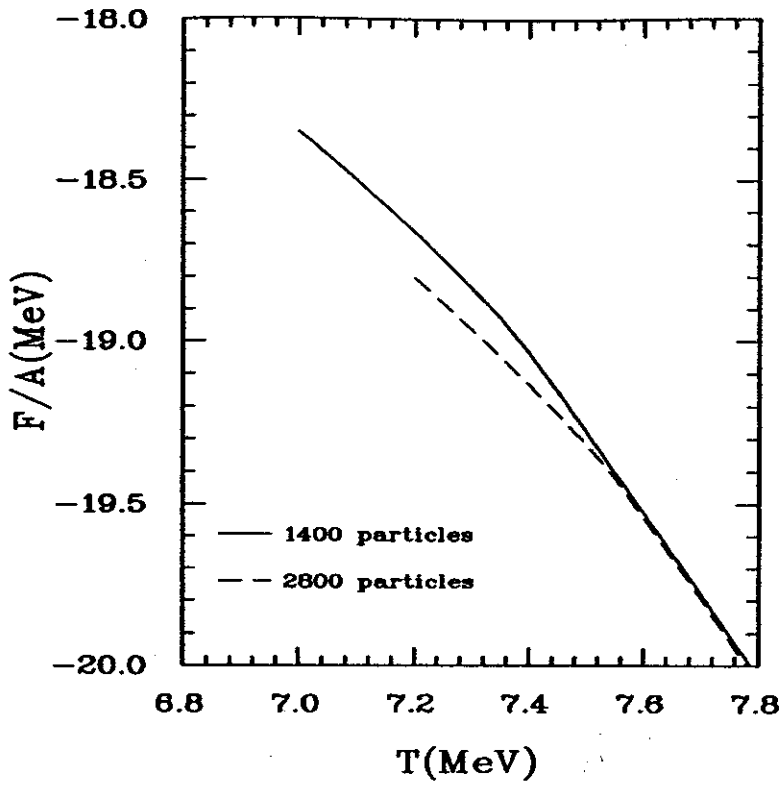

Fig.18. The first derivative of the free energy per particle ($-TlnQ_A/A$) will show a break as a function of temperature for a large system. Shown here are cases of 1400 and 2800 particles.

We follow this up in Fig.19 by calculations of specific heat C_v per particle for 200, 1400 and 2800 particles. As the number of particles increases, the maximum in the C_v per particle becomes sharper and the height increases. In Fig.20 we have tried to understand the origin of this singularity in greater detail. Let us denote by $< a_{max} >$ the ensemble average of the mass number of the heaviest composite (the technique for this calculation is given in [121]). This should scale like A where A is the number of particles in the disintegrating system. In Fig.20 we have plotted $< a_{max} > /A$ as a function of T/T_b where T_b is the temperature at which the specific heat maximises. As A becomes large, the drop in the value of $< a_{max} > /A$ at $T = T_b$ becomes sharp. The sudden disappearence of this large blob of size $\approx A/2$ causes this behaviour of C_v.

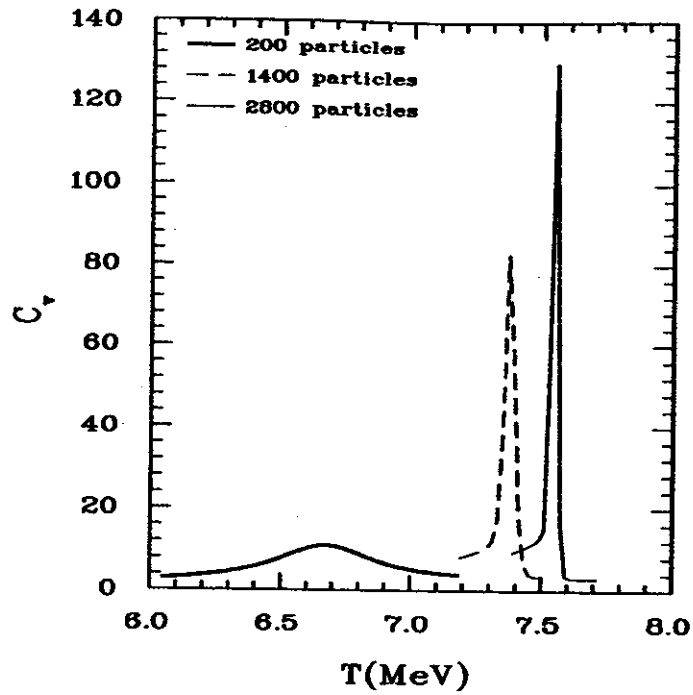

Fig.19. As the number of particles increase, the maximum in C_v per particle becomes very narrow and very high.

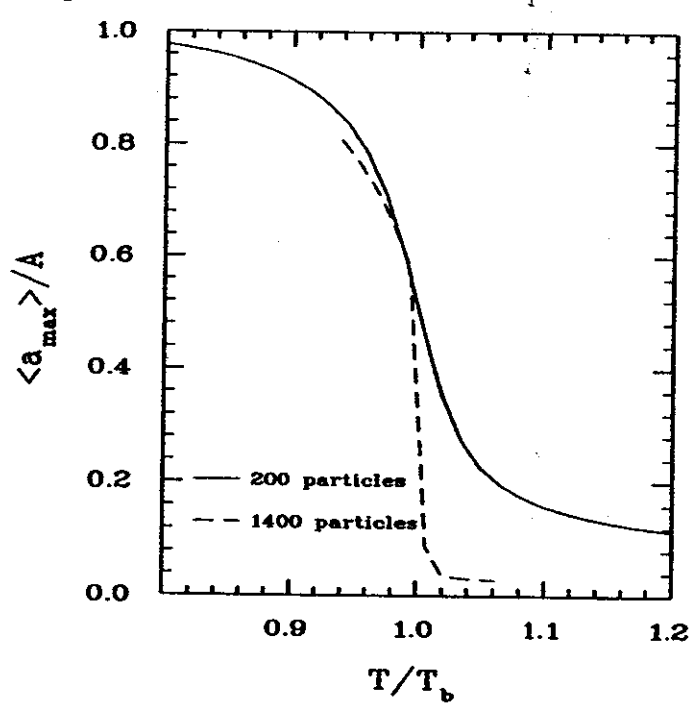

Fig.20. For large systems a large blob of matter suddenly disappears at T_b.

In Fig.21 we have drawn a $p-\rho$ diagram for a system of 200 particles at various temperatures. We have also drawn a line that is labelled co-existence which passes through the points where the specific heat attains the highest values. For plotting this graph we have used $V_{ex} = 200/\rho_0$. We stop below ρ/ρ_0=0.50. At higher density the approximation of non-interacting clusters (even after including Van der Waals type correction for finite volumes

of the composites) would be very questionable.

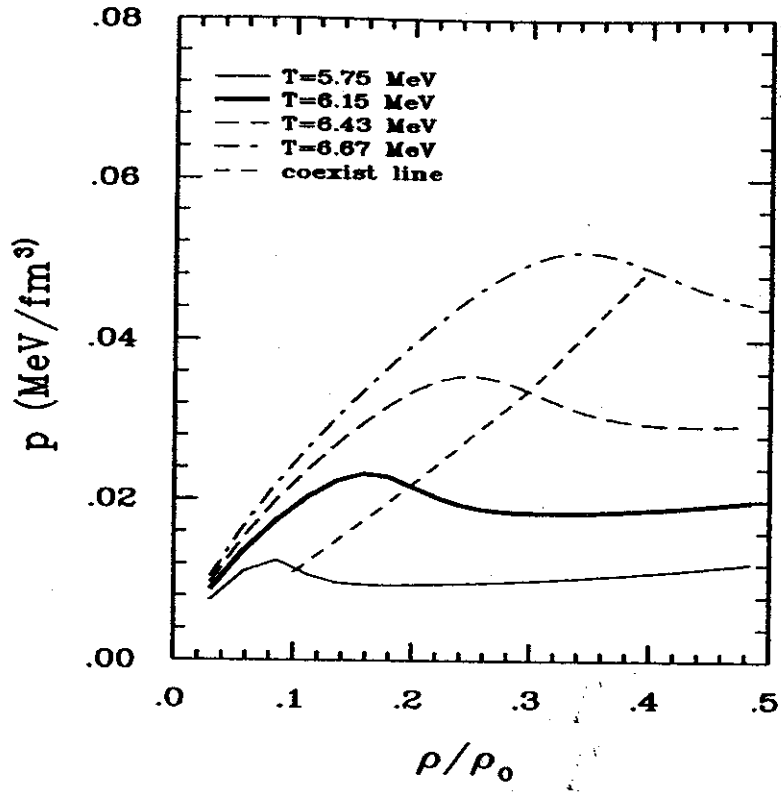

Fig.21. Isotherms for different temperatures for a system of 200 nucleons. Here it is assumed that $V_{ex} = 200/\rho_0$. Line labelled coexistence goes through points of highest C_v.

One approximation in the above calculation is the assumption of constant excluded volume. The excluded volume (as can be verified in Monte-Carlo simulation) is a function of the total multiplicity . It is also a function of the freeze-out volume inside which the particles are constrained to move. For 200 particles, the effect of this variability of the excluded volume on the $p - V$ diagram was investigated in [123]. The difference is not large. However, this has not been studied in the thermodynamic limit. It will be very interesting to investigate what effect it will have on the nature of the phase transition in the very large A limit.

The thermodynamic properties of this model have been further studied in [124,125].

XII. GENERALISATION TO A MORE REALISTIC MODEL

For comparisons with actual data the model must be made more realistic. Towards that goal, a composite is now labelled by two indices: $\omega \rightarrow \omega_{i,j}$ where the the first index in the subscript refers to the number of protons and the second, to the number of neutrons in the composite. The partition function for a system with Z protons and N neutrons is given by

$$Q_{Z,N} = \sum \Pi_{i,j} \frac{\omega_{i,j}^{n_{i,j}}}{n_{i,j}!} \tag{12.1}$$

There are two constraints: $Z = \sum i \times n_{i,j}$ and $N = \sum j \times n_{i,j}$. These lead to two recursion relations any one of which can be used. For example,

$$Q_{Z,N} = \frac{1}{z} \sum_{i,j} i\omega_{i,j} Q_{Z-i,N-j} \tag{12.2}$$

where

$$\omega_{i,j} = \frac{V}{h^3}(2\pi mT)^{3/2}(i+j)^{3/2} \times q_{i,j} \tag{12.3}$$

Here $q_{i,j}$ is the internal partition function. These could be taken from experimental binding energies, excited states and some model for the continuum or from the liquid drop model or a combination of both. The versatility of the model lies in being able to accommodate any choices for $q_{i,j}$. A choice of $q_{i,j}$ from a combination of the liquid-drop model for binding energies and the Fermi-gas model for excited states that has been used is

$$q_{i,j} = \exp[(W_0(i+j) - \sigma(i+j)^{2/3} - \kappa\frac{i^2}{(i+j)^{1/3}} - s\frac{(i-j)^2}{i+j} + T^2(i+j)/\epsilon_0)/T] \tag{12.4}$$

where W_0=15.8 MeV, σ=18.0 MeV, κ=0.72 MeV and ϵ_0= 16 MeV. One can recognise in the parametrisation above the volume term, the surface tension term, the Coulomb energy term, the symmetry energy term and contributions from excited states.

The coulomb interaction is long range; some effects of the Coulomb interaction between different composites can be included in an approximation called the Wigner-Seitz approximation. We assume, as usual, that the break up into different composites occurs at a radius R_c which is greater than normal radius R_0. Considering this as a process in which a uniform dilute charge distribution within radius R_c collapses successively into denser blobs of proper radius $R_{i,j}$ we write the Coulomb energy [126] as

$$E_C = \frac{3}{5}\frac{Z^2e^2}{R_c} + \sum_{i,j}\frac{3}{5}\frac{i^2e^2}{R_{i,j}}(1 - R_0/R_c) \tag{12.5}$$

It is seen that the expression is exact in two extreme limits: very large freeze-out volume ($R_c \to \infty$) or if the freeze-out volume is the normal nuclear volume so that one has just one nucleus with the proper radius.

For the thermodynamic model that we have been pursuing, the constant term $\frac{3}{5}\frac{Z^2e^2}{R_c}$ in the above equation is of no significance since the freeze-out volume is assumed to be constant. In a mean-field sense then one would just replace the Coulomb term in Eq.(12.4) by $\kappa\frac{i^2}{(i+j)^{1/3}}(1.0 - (\rho/\rho_0)^{1/3})$

Calculations with the thermodynamic model with two kinds of particles and realistic $q_{i,j}$ were done in [127,128]. A plateau in the caloric curve is found around 5 MeV which is in accordance with experimental finding. An interesting point in the calculation is the following observation. Without the Coulomb, the height in the peak of the specific heat increases with A (see previous section). With Coulomb the height is reduced and the dependence on A nearly disappears. The growth in size is compensated by the growth in Coulomb repulsion. This means the caloric curve is approximately universal,i.e., does not depend strongly on

the specific system which is disintegrating. We show the caloric curves computed for three disintegrating systems in Fig.22. This is taken from [127].

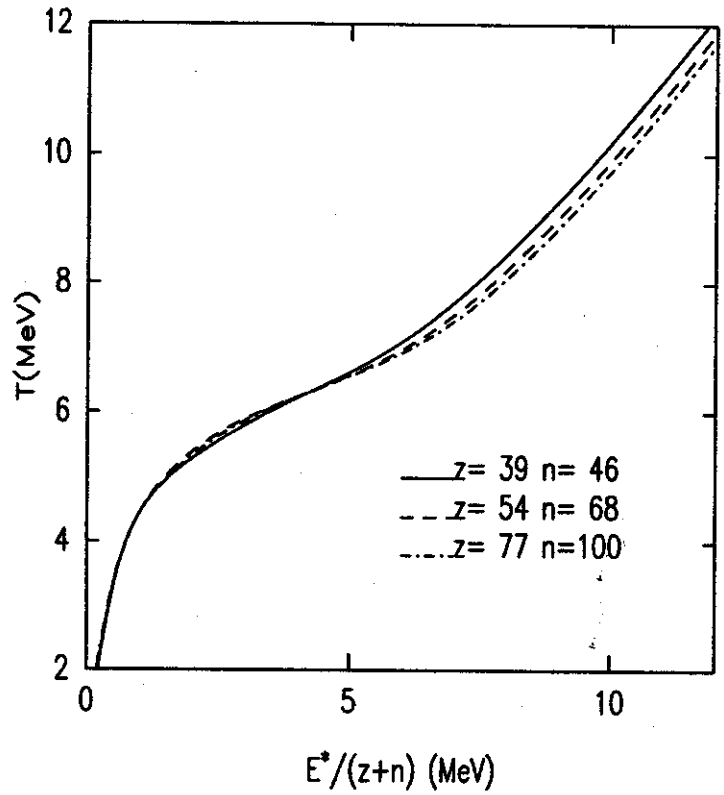

Fig.22. The caloric curve for three different nuclei. The Coulomb interaction is included in the Wigner-Seitz approximation.

Of course, the model can also be used to calculate other observables, not necessarily related with any phase transition aspect. However, for many purposes an "afterburner" calculation is required. The composites obtained in the calculations are "hot". They will subsequently decay by particle emissions. In [129] these subsequent decays were included in an approximate manner so that one can compare with experimental yields of boron, carbon and nitrogen isotopes. This comparison is shown in Fig.23.

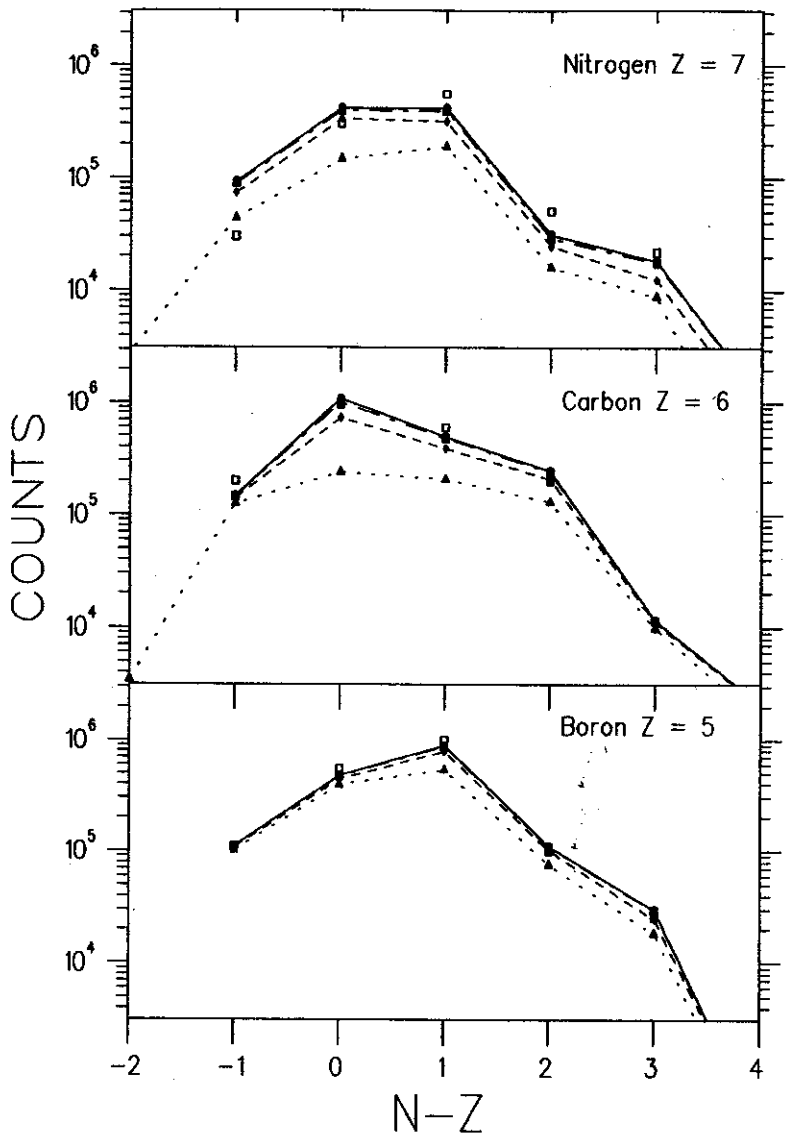

Fig.23. Neutron number (N), proton number (Z) vs. counts for the three cases of boron, carbon and nitrogen. The experimental data are from [130] S+Ag at 22.3A MeV. The open squares are the experimental data. The dotted line with the triangle plotting symbol is the thermodynamic model calculation as described in the text. A temperature of 5 MeV is used. The other curves are obtained by allowing sequential decays of hot nuclei. The calculation stops after four possible decays (the solid line) as virtually no changes are seen between triple and quadruple decays.

XIII. A BRIEF REVIEW OF THE SMM MODEL

A very comprehensive review of this model exists [102] so we only give a brief resumé here. It is relevant to mention that a peak in the specific heat at about 5 MeV temperature was predicted in the model well before experiments were done [131].

In the SMM each break-up channel is treated separately. A given channel is specified by the set of $n_{i,j}$'s, V and temperature T. The volume V which is the free volume available for the motion of the cms of the composites is taken to be $V = \chi V_0 = \chi A/\rho_0$ where χ is multiplicity dependent ($M = \sum n_{i,j}$).

$$\chi = (1 + \frac{d}{r_0 A^{1/3}}(M^{1/3} - 1))^3 - 1 \tag{13.1}$$

In the above d is taken to be 1.4 fm; $r_0 A^{1/3}$ is the normal radius of a nucleus of A nucleons. The concept of temperature is used but its primary use is to make the energy in each channel the same value and to correspond to the experimental situation. It is therefore a microcanonical calculation in spirit. The energy in a given channel E_{tot} is given by

$$E_{tot}(T, V) = E^{tr}(T) + \sum E_{i,j}(T) n_{i,j} + E_{cou}(V) \tag{13.2}$$

where $E^{tr}(T) = \frac{3}{2}(M - 1)T$, $E_{i,j}(T)$ gives the intrinsic energies at temperature T (includes binding energies, contribution from excited states etc.; see the discussion in section XII) and $E_{cou}(V)$ completes the Wigner-Seitz estimation of Coulomb energy. The crucial thing here is the choice of channels. It is impossible to include all channels. For A=200 the number of possible multifragment partitions is 3.9×10^{12} so a Monte-Carlo sampling which is geared to include the most important channels at a given excitation energy is needed. This is a very elaborate story in itself and all we can do here is to provide references. An important paper which elaborates on the procedure is [132]. The review article on the model [102] gives a more complete list of references. As in all models of this type, sequential decays of the hot fragments need to be included to compare with most experimental data. The fit with data on IMF multiplicity, mean energy etc. is normally quite good.

XIV. THE MICROCANONICAL APPROACH

Pioneers of this approach were the Berlin group [133] and Randrup and collaborators [116]. In the Berlin approach, the clusters, which have finite sizes, are all totally inside the freeze-out volume. This freeze-out volume is the same for all channels. Randrup et al. demand that centres of all the clusters should be within the freeze-out volume. There are other practical differences between the two formulations. Let us sketch the general procedures that any microcanonical calculation will have to accomplish. Suppose that we are interested only in calculating the average number of clusters of a composite which has k protons and l neutrons, i.e., $< n_{k,l} >$, when the total energy is E and the disintegrating system has Z protons and N neutrons. How do we proceed? For simplicity we will say that the only interaction between the clusters is that they can not overlap. We will also assume that the composites have only ground state.

There are many possible break-up channels. All divisions (that satisfy $\sum i n_{i,j} = Z$ and $\sum j n_{i,j} = N$ where $n_{i,j}$ is the number of cluster which has i protons and j neutrons) are allowed and equally likely to occur. The phase space available to each channel, however, will be, in general, different and will strongly affect the final result. The phase space associated with each break-up channel is

$$\Omega[n_{i,j}] = \frac{1}{h^{3M}} \Pi_{p,q} \frac{1}{n_{p,q}!} \int \Pi d^3 r_{i,j} d^3 p_{i,j} \delta[E + \sum B_{i,j} - \sum p_{i,j}^2/2m_{i,j} - \sum v(i,j:m,n)] \quad (14.1)$$

Here M is the multiplicity in the channel $[n_{i,j}]$, $B_{i,j}$ the binding energy of the cluster (i,j) and $v(i,j:m,n)$ is the potential energy between the clusters (i,j) and (m,n). In our case it is either 0 (when they are separated) or ∞ (when they overlap). The momentum integral is analytic:

$$\int d^3 p_1 .... d^3 p_f \delta[K - \sum_1^f \frac{p_i^2}{2m_i}] = \frac{2\pi}{\Gamma(3f/2)} (m_1 .... m_f)^{3/2} (2\pi K)^{3f/2-1} \quad (14.2)$$

Once the momentum integral is done we still need to do the configuration space integral. This is by no means trivial but one can estimate it in a Monte-Carlo procedure. The first particle is placed at a random position inside the freeze-out volume. Having placed the first one we try to place the second one, again at a random position in the freeze-out volume. We may succeed but we may fail also if, by chance, the second chosen position was such that the new particle overlaps with the particle already in. A successful run occurs if we are able to put M particles in without failing once. An unsuccessful run happens if anytime in the chain we failed to put a particle. Then the volume integral is $(V_{freeze-out})^M \times \frac{N_s}{N_{un}+N_s}$ where N_s is the number of successful runs and N_{un} is the number of unsuccessful runs. The quantity just calculated is V^M where V is the volume of the thermodynamic model.

Provided all this is done for each channel and we have calculated the phase space $\Omega[n_{i,j}]$ for each channel, the average number of particles of a composite with k protons and l neutrons will be given by $\sum n_{k,l} \Omega[n_{i,j}] / \sum \Omega[n_{i,j}]$ where $n_{k,l}$ is the number of composites with proton number k, neutron number l in the channel labelled by $[n_{i,j}]$ and $\Omega[n_{i,j}]$ is the phase space integral associated with this channel. The sum is over all $[n_{i,j}]$.

In practice, this procedure is impossible to carry out as the number of channels is inordinately large. An "importance sampling" [134] of the phase space is necessary. This is usually done with the Metropolis method [134,135]. We will have occasion to use this technique later also. One attempts elementary moves by which one migrates from one channel (here with multiplicity M) to a neighbouring channel (multiplicity $M+1$ or $M-1$). These moves are "fission" (take a composite and arbitrarily break it into two pieces) and "fusion" (join two composites). Let us call Ω the phase space integral before the move. One also calculates the phase space integral after the attempted move. Let us call this Ω'. If $\Omega' > \Omega$ the move is accepted. If $\Omega' < \Omega$, the probability of switching is given by the ratio Ω'/Ω (see [134] why these give the correct transition probabilities). An event is accepted every N attempted moves (some successful and some not) and averages will be calculated with many such events; N should be sufficiently large to avoid event-to-event correlation and of course one should have sufficient number of events to reduce statistical errors.

There are a great many details which need to be worked out before such a program can be instituted for practical calculations. The interested reader should consult the original literature. The techniques for microcanonical calculations were developed in the mid eighties spanning several papers, each one an improvement over the previous one. What we have outlined here are the general principles.

XV. THE PERCOLATION MODEL

This model is strikingly different from the models described above. The model has been extensively studied in condensed matter physics. A delightful monograph exists [96] which has all the material needed to follow the application in nuclear physics. The applications in nuclear physics were made by Campi and collaborators [92,94] and by Bauer and collaborators [93,95].

There are two types of percolation models: site percolation and bond percolation. For applications to nuclear physics, bond percolation was used. In bond percolation there are N lattice sites. One uses a three-dimensional cubic lattice, thus $N = 5^3, 6^3$ etc. The number of nucleons is also N. Each lattice site contains one nucleon. We do not distinguish between neutrons and protons. The crucial parameter is the bonding probability p whose value can vary between 0 and 1. The probability that two nearest neighbour nucleons will be part of a cluster is given by the value of p. If p=0 (high excitation energy) all N^3 nucleons will emerge as singles. If p=1, the nucleons stay together as one nucleus (low excitation energy, not enough to break up the nucleus). For the values of p between the two extremes Monte-Carlo sampling is needed to generate events and determine in each event the occurrence of clusters of different sizes. There is a phase transition in this model. One can define a percolating cluster; this is a cluster, which, if it exists, spans the walls, i.e., connects opposite walls through an unbroken cluster. For N very large, this appears at the value of $p = 0.2488$. This value of p will be labelled by p_c. The order parameter in this model is the probability that an arbitrary site (equivalently an arbitrary nucleon) is part of this percolating cluster. Below p_c, this is zero since there is no percolating cluster. It starts from zero at p_c and continuously moves towards the value 1 as the value of p is increased. The phase transition in this model is continuous and not a first-order phase transition. This aspect had a very important and strong influence in the history of search for phase transition in heavy-ion collisions. Near critical points, One can define critical exponents and try to evaluate them from experiment. We will see later that even though we now regard the phase transition in nuclear heavy ion collisions to be first order, it is meaningful to try to measure certain exponents. In the lattice gas model (to be described below) these retain significance even when one is far from a critical point and is in the vicinity of a first-order phase transition.

We give the values of the more common exponents in the thermodynamic limit (i.e., $N \to \infty$). One of these exponents we have already encountered many times. Near the critical point the yield of mass a is given by

$$Y(a,p) = a^{-\tau} f[(p - p_c)a^{\sigma}] \tag{15.1}$$

At the critical point the yield is a power law. The value of τ in the percolation model is 2.18. The value of σ in the above equation is 0.45. Let us denote the mass of the largest cluster by a_{max}. The second moment is defined by

$$S_2 = \sum{}' a^2 Y(a)/A \tag{15.2}$$

Here the summation excludes the a_{max} and $A = N^3$ is the number of nucleons. The second moment S_2 diverges: $S_2 \propto |p - p_c|^{-\gamma}$ where the value of γ is 1.80. In finite systems S_2 will not become infinite but will go through a maximum as p_c is traversed. Above the percolation point the order parameter is given by $a_{max}/A \propto |p - p_c|^{\beta}$ where $\beta = 0.18$.

In spite of its simplicity, the percolation model was an aid in understanding various phenomena. It has now been replaced by a lattice gas model which is more realistic, more versatile and indeed contains the percolation model as a special case.

XVI. THE LATTICE GAS MODEL (LGM)

The advantage of the percolation model is that clusters are easily obtained. This break-up can be compared with experiment. But there is no equation of state in the usual sense. The equation of state requires two variables: p and V, then T is automatically known from the EOS: or p and T then the EOS gives V etc. There is only one parameter in the percolation model, the bond probability. There is no obvious way this model can be linked to finite temperature Hartree-Fock theory or the thermodynamic model or SMM or the microcanonical model. There is no Hamiltonian.

In [88,89] LGM was introduced so that one has an EOS as in Hartree-Fock theory but also has the capability of predicting clusters as in the percolation model. The EOS of LGM in mean-field theory in a grand canonical ensemble is done in textbooks [13]. To obtain clusters in the model an extension of the wellknown model is necessary. Although LGM today is more complete with the inclusion of isospin dependence and Coulomb interaction, we introduce first the simplest version. This will be very easily generalised later.

As in percolation, we have N_s lattice sites but now, in general, N_s is greater than A, the number of nucleons that need to be put in these sites. When $N_s = A$ the nucleus has normal density. We are not allowed to put more than one nucleon on a site. Thus the model is limited to normal volume or larger. Because cluster formation presumably takes place in a volume significantly larger than normal volume, this restriction is not debilitating. The nearest neighbours have a bond ϵ which is negative. Only nearest neighbours interact. The exclusion of the possibility of two nucleons occupying the same site mimics a short range repulsion. The attractive nearest neighbour interaction simulates the attractive interaction which is also short range (but longer than the short range repulsive interaction).

Let N_{nn} be the number of nn bonds in a specific lattice configuration. The energy carried by these bonds is ϵN_{nn}. Thus the partition function is

$$Q = \sum_{N_{nn}} g(N_s, A, N_{nn}) e^{-\beta \epsilon N_{nn}} \tag{16.1}$$

Here $g(N_s, A, N_{nn})$ is the number of configurations which have N_{nn} nearest neighbour bonds and which can be formed from A nucleons in N_s lattice sites. This is not analytically solvable. Hence calculation of observables where configurations have the above weighting requires Monte-Carlo simulations.

The simulations are usually done in the Metropolis algorithm. Starting from an initial configuration chosen suitably [109], one attempts a switch between an unoccupied site and an occupied site. If the resulting change of energy ΔE is negative, the switch is accepted. If ΔE is positive, it is accepted with a probability $e^{-\Delta E/T}$. After a large number N of attempted switches (some successful and some unsuccessful) an event is accepted. N should be large enough to avoid event to event correlation.

The grand canonical ensemble of the LGM (sum over all possible A's) can be mapped onto a three dimensional Ising model [13,136]. The latter has been extensively studied and

indeed serves as a model for liquid-gas phase transition. Many of the known results of the Ising model can be directly applied. For example in the large A limit the critical temperature will be 1.1275ϵ and the critical density $\rho/\rho_0 = A/N_s = 0.5$.

We consider now an extension of the model so that clusters can be computed. Suppose we have generated a configuration. At finite temperature, the nucleons will not be frozen at the lattice sites. They will have momenta. In this configuration each of the A nucleons can be given a momentum by Monte-Carlo sampling of a Maxwell-Boltzmann distribution at the given temperature. Thus in an event we have nucleons at definite lattice sites with definite momenta. There may be some isolated nucleons which have no nearest neighbours. These clearly are monomers. The next case is when there is a cluster of two nucleons which are nearest neighbours of each other. They will form a bound cluster of two if the kinetic energy of relative motion is insufficient to overcome the attraction between the two nucleons, i.e., $p_r^2(1,2)/2\mu + \epsilon < 0$. Here $\vec{p}_r(1,2) = \frac{1}{2}(\vec{p}_1 - \vec{p}_2)$ and $\mu = m/2(m$=mass of one nucleon).

It turns out that this prescription which is rigorously correct for a cluster of two also works *statistically* for larger clusters. That is, we can formulate a rule that independent of other neighbours, two nearest neighbours form part of the same cluster if the relative kinetic energy of the two is insufficient to overcome their attraction. It is obvious that this recipe, introduced in [88,89], reduces the many body problem of recognising a cluster of many nucleons into a sum of independent two body problems. For brevity we refer to this as PD recipe. To see why this works *statistically* even if not individually let us specifically consider a three body cluster [109].

For three particle clusters, nearest neighbours are either linear or L shaped. In either case there is only one particle which has two bonds (label this by particle 2) and two others (label them 1 and 3) which have one bond each. According to the PD recipe this will form a three body cluster if $p_r^2(1,2)/2\mu + \epsilon < 0$ and $p_r^2(2,3)/2\mu + \epsilon < 0$. To check if particle 3 is part of a three body cluster (similar arguments will be needed for particles 1 and 2) we should instead verify if $p_r^2(12,3)/2\tilde{\mu} + \epsilon < 0$. Here $\vec{p}_r(12,3)$ is the relative momentum between the centre of mass of (1+2) and 3; $\tilde{\mu} = (2/3)m$ is the reduced mass for this relative motion. Thus there may be cases where the PD recipe gives a three body cluster wheras in reality the third one will separate. But there will also be cases where the PD recipe will deem that the third one will separate whereas in reality it stays attached. Statistically overestimation will cancel out underestimation because for a Maxwell-Boltzmann distribution all relative motions are also Maxwellian at the same temperature. That is, in Monte-Carlo simulation, $p_r^2(12,3)/2\tilde{\mu}$ will be as many times below the value $-\epsilon$ as $p_r^2(2,3)/2\mu$ will be.

The same argument applies to particle 1. For particle 2. it can be verified that if $p_r^2(1,2)/2\mu + \epsilon < 0$ and $p_r^2(2,3)/2\mu + \epsilon < 0$ then $p_r^2(13,2)/2\tilde{\mu} + 2\epsilon < 0$ is always satisfied.

Campi and Krivine have used a different approach and come to the conclusion [137] that the PD recipe gives the correct number of particle stable clusters.

Recognition of clusters in a many body system is a complicated issue. The PD recipe was tested in [138] in numerical simulations and found reliable. In the PD recipe once the configuration of A nucleons and their momenta are given, the cluster decomposition is immediate. One may however, starting from this initial condition, switch to a different model. One may propagate particles using molecular dynamics. At asymptotic times clusters are easily identified as different clusters will separate from each other. Of course the result will depend upon the interaction potential used for molecular dynamics propagation. To test

the PD recipe one must use an interaction consistent with the assumptions of the lattice gas model. Let a be the length of each side of the elementary cubic lattice. The interaction between particles must become repulsive when the distance between them gets to be less than a. At distance $\sqrt{2}a$ it is deepest at -5.33 MeV. At distance beyond it must go to zero rapidly. Given the same initialisation and such interaction, molecular dynamics produced very similar results as the PD recipe.

It follows that with this recipe of calculating composites, we do not need to worry about subsequent evaporation as one needs to in many other models; thermodynamic, SMM and microcanonical. This is a tremendous advantage. Evaporation was already taken into account when we applied the PD recipe. One does not take the size of the cluster to be given by just the number of nucleons which are connected to each other through the nearest interaction [139]. Some of these will fly away. The rest that remain and are counted, are particle stable.

With a prescription for obtaining clusters, the LGM will show many features in common with the percolation model. This leads to interesting properties.

XVII. PHASE TRANSITION IN LGM

Whether one later ascribes momenta to nucleons and calculates clusters or not, there is phase transition in the traditional LGM. The thermodynamics of the system does not depend upon the definition of clusters. The coexistence curve can be drawn. This diagram is simply transferable from studies in the three dimensional Ising model. We show this in Fig.24. The thermal critical point is shown in the diagram as C.P.

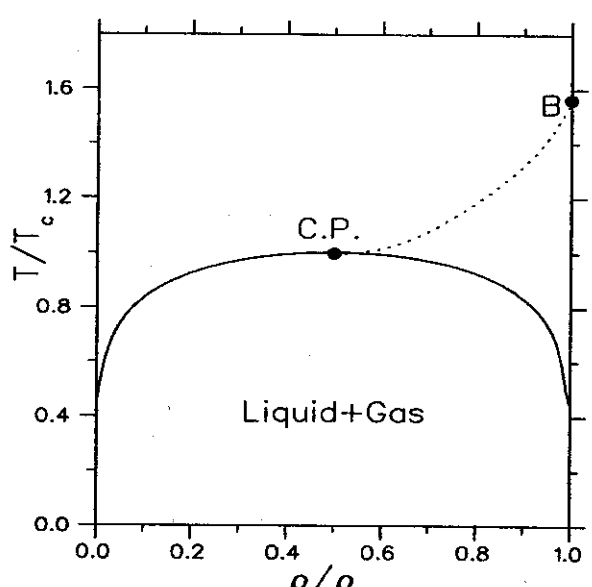

Fig.24. Phase diagram of the three dimensional lattice gas model. The full line is the coexistence curve. Percolation sets in along the dotted line and continues along the coexistence line to the left of C.P.

With a rule for calculating clusters it will be very interesting if the thermal critical point also coincides with the onset of a percolating cluster. This aspect was studied by Coniglio

and Klein [140]. They propose that the probability that two nearest bonds have an active bond between them be given by

$$p = 1 - \exp(-\beta|\epsilon|/2) \tag{17.1}$$

With this definition, these authors, using renormalisation group techniques, proved that at (ρ_c, T_c) percolation just sets in. However, percolation sets in not just at the thermodynamic critical point but rather along a continuous line in the (ρ, T) plane (the dotted line in Fig.24). This was studied in [141] and the line is called Kertész line. Thus the critical exponents τ, β and γ are meaningful not only at the critical point but along an entire line.

It turns out the PD recipe which is a natural choice for calculation of clusters in the case of nuclear disintegration is very close to the Coniglio-Klein (CK) formulation. The PD formula for p (using the fact that in a Maxwell-Boltzmann distribution the relative motion is also Maxwell-Boltzmann) is

$$p = 1 - \frac{4\pi}{(2\pi\mu T)^{3/2}} \int_{\sqrt{2\mu|\epsilon|}}^{\infty} \exp(-p_r^2/2\mu T) p_r^2 dp_r = 1 - \frac{2}{\sqrt{\pi}} \int_{|\epsilon|/T}^{\infty} e^{-q} q^{1/2} dq$$

A comparison of p according to the above formula to the Coniglio-Klein formula is shown in Fig.25. They are very close. As far as we know, all cluster calculations in nuclear physics use the PD recipe.

With the aid of Fig.24 we can now discuss phase transition in nuclear disintegration according to LGM. The freeze-out volume that fits the data best [89] is bigger than twice the normal nuclear volume. In that case as the temperature of the disintegrating system is raised from a low value to a high value (either by changing the beam energy or by gating on appropriate impact parameter) the system will cross the coexistence curve on the low density side of the critical point (to the left of C.P. in Fig.24). Thus we will have first-order phase transition [142]. As the line is crossed one will see a discontinuity in specific heat, a peak in S_2 and other features.

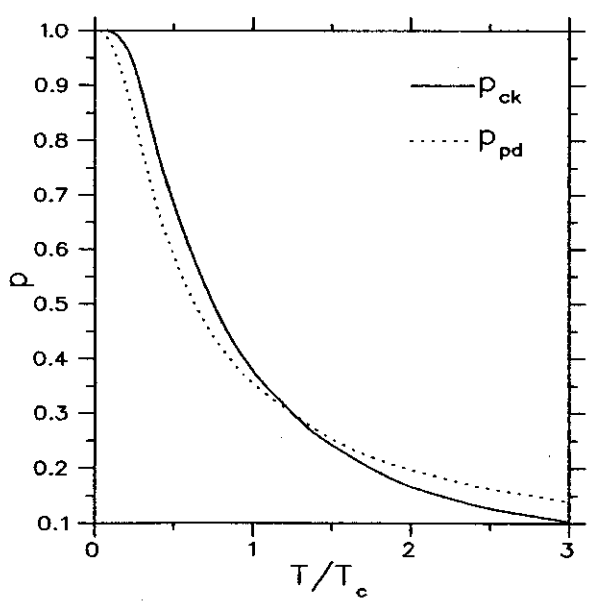

Fig.25. The bond probability p is plotted as a function of temperature. The solid line (p_{ck}) is the Coniglio-Klein formula, the dotted line (p_{pd}) is the PD recipe.

XVIII. ISOSPIN DEPENDENT LGM INCLUDING COULOMB INTERACTION

For many practical applications, it becomes necessary to distinguish between like particle interactions (bond between proton and proton or/and between neutron and neutron) and unlike particle interaction (bond between neutron and proton); ϵ between like particles must be repulsive or zero otherwise we can obtain dineutron or diproton bound states. The bond between unlike particles will be attractive. At zero temperature in nuclear matter, energy considerations imply that sites will be alternately populated by neutrons and protons. Thus the only nearest neighbour interactions will be those between unlike particles. Nuclear matter binding energy then dictates that $\epsilon_{np} = -5.33$MeV. This however does not fix the value of ϵ_{pp} or ϵ_{nn}.

It is clear that the Monte-Carlo technique of generating events for finite nuclear systems can also be used when the interactions between like and unlike particles are different. The Coulomb interaction between protons can also be included. When this is done at zero temperature we obtain the ground state energies. This was done in [109] for a range of nuclei for $\epsilon_{pp} = \epsilon_{nn} = 0$. The binding energies of these nuclei thus computed were then fitted to a simple liquid-drop mass formula:

$$E/A = -a_v(1 - \kappa I^2) + a_s(1 - \kappa I^2)A^{-1/3} + a_c\frac{Z^2}{A^{4/3}} \tag{18.1}$$

Here $I = (N-Z)/A$ is the neutron-proton asymmetry of the nucleus. The fit of LGM binding energies to this four parameter formula is quite good. We compare the four parameters deduced from LGM to liquid-drop model values [143] in the table. Considering the simplicity of the model, the agreement is gratifying. We also notice that the asymmetry parameter κ is larger than the liquid-drop value. Since ϵ_{np} is fixed from nuclear matter binding energy, the only way we can bring down κ is to make ϵ_{pp} and ϵ_{nn} go negative. As explained already this is not permissible. We are therefore led to the conclusion that $\epsilon_{np} = -5.33$MeV and $\epsilon_{pp} = \epsilon_{nn} = 0$ are the best choices for isospin dependent LGM.

Table I. Lattice gas and phenomenological liquid-drop model parameters.

Model	a_v	a_s	κ	a_c
LGM	16.0	16.03	2.14	0.746
Phenomenological	15.68	18.56	1.79	0.717

XIX. CALCULATIONS WITH ISOSPIN DEPENDENT LGM

We mentioned earlier that the isotopic content of the gas phase can be different from that of the liquid phase. This comes out nicely in LGM. Fig.26, taken from [109] demonstrates this. Here one considers breakup of ^{197}Au at different temperatures. The average value of the charge of the largest residue at each temperature is denoted by $< Z_{max} >$. This will drop in value as the temperature is increased. Also calculated is the average value of neutron content

$< N_{max} >$ of the largest cluster. We may regard the largest cluster as the liquid phase and the rest of the nucleons as primarily belonging to the gas phase. The disintegrating system has $N/Z = 1.49$. With an isospin dependent LGM, the $< N_{max} > / < Z_{max} >$ is much closer to 1. This means the gas phase has a higher N/Z ratio, higher than that of the parent system. The reason for this behaviour is that the symmetry energy drives the N/Z ratio of the largest cluster towards the value unity. The Coulomb effect will offset this as shown in the figure. The simplest version of the LGM which had no isospin dependence and no Coulomb term will keep the $< N_{max} > / < Z_{max} >$ at the value pertaining to the disintegrating system. This is also shown in the figure. This contradicts experiment.

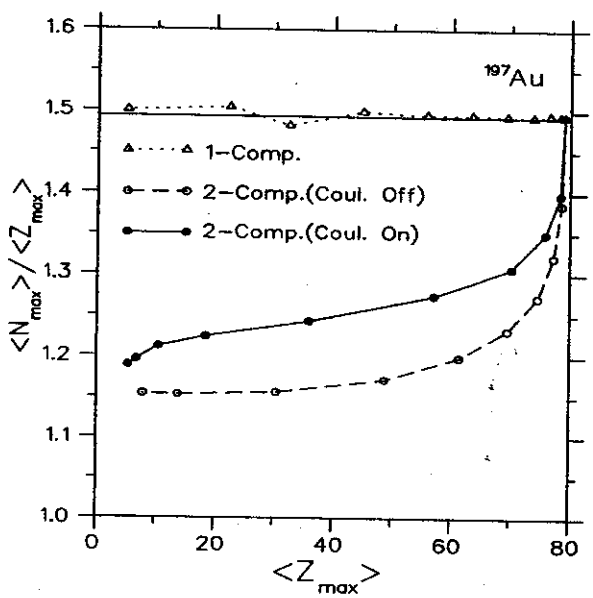

Fig.26 The ratio $< N_{max} > / < Z_{max} >$ as $< Z_{max} >$ changes (because temperature changes). The temperature increases by 0.5 MeV between two successive symbols as we move from right to left starting with 2.5 MeV.

For ^{197}Au we show several quantities as a function of temperature. In experiments one extracts the quantity τ where the yield $Y(Z)$ as a function of Z is fitted to $Y(Z) \propto Z^{-\tau}$. The power law comes out quite well in LGM. We notice that the maximum in C_v, the maximum in S_2 and the minimum in τ all bunch around T=4.2 MeV which we then associate with the crossing of the coexistence curve. The maximum in N_{IMF} is at a slightly higher temperature.

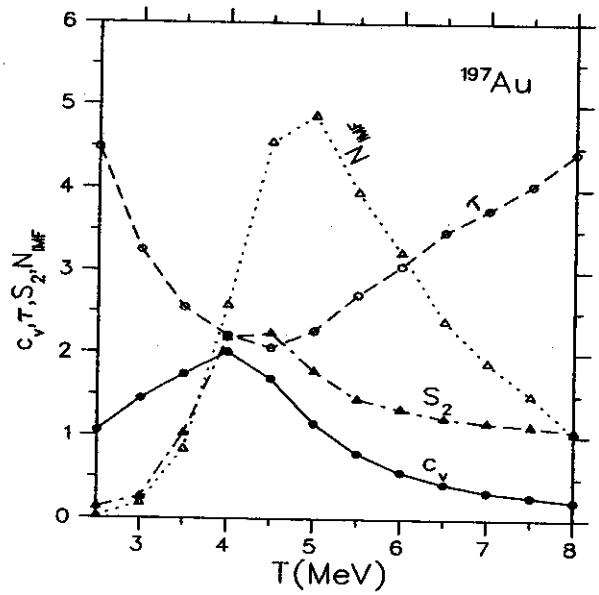

Fig.27 The specific heat C_v, the exponent τ for the power law fit to the yields of isotopes, the second moment S_2 and the IMF yield are shown as a function of temperature for ^{197}Au. The calculations are done in an 8^3 lattice.

The EOS for isospin dependent LGM in mean-field theory using the Bragg-Williams and the Bethe-Peierls approximation can be found in [144]. Phase transition aspects, much more than what we have covered here, can be found in [108,145–147]. The model has been used successfully to obtain several experimental results, for example, $t/^3He$ ratios as the isotopic content of the parent system changes [108,109]. Some applications were made in [110]. The shortcomings of the model for detailed fittings to experimental data are obvious. The model has cubical symmetry rather than spherical symmetry. The shell effects are missing although the smooth part of binding energy is approximately reproduced. The excitation spectrum of the composites is incorrect. But it has many nice features not present in other models. Here composites are formed directly out of fluctuations. One starts with interactions between two nucleons. The inclusion of Coulomb effects is precise, though numerical. Best of all, it includes interactions between composites.

XX. FRAGMENT YIELDS FROM A MODEL OF NUCLEATION

A phenomenological droplet model based on homogeneous nucleation theory has also been used to describe mass yields provided in heavy-ion collisions [148]. The nucleation model is an extension of the Fisher droplet model which was originally used to describe such yields. The extension allows for the possibility that supersaturated systems are produced during the brief encounter of two colliding nuclei. Homogeneous nucleation occurs in supersaturated systems when chance collisions of particles in the gas phase yield to local density inhomogeneties. These inhomogenities are droplets of particles of the liquid phase that will grow in size if the systems lived for a long time. Specifically, in the supersaturated phase, a critical size droplet exists which is determined by the surface tension and the difference of liquid and gas chemical potentials. Droplets larger than the critical size will grow by accumulating nucleons in order to lower the free energy of the system while droplets of smaller

size will evaporate nucleons also lowering the free energy of the system. This behaviour in growth and evaporation reflects itself in a yield distribution which is U-shaped with an initial decrease with A until the critical size A_c is reached and then an increase in yield with A above A_c. In this nucleation description, the probability of formation of droplets is determined by calculating the change in Gibbs free energy with and without a drop at constant temperature and pressure. For example, if a droplet of size A is surrounded by B droplets of the gas phase, then $G_{withdrop} = \mu_l A + \mu_g B + 4\pi R^2 \sigma(T) + T\tau lnA$ and $G_{nodrop} = \mu_g(A+B)$. Here μ_l and μ_g are the liquid and gas chemical potentials, R is the radius of the drop (with $R = r_0 A^{1/3}$) and $\sigma(T)$ is the surface free energy such that $4\pi r_0^2 \sigma(T) = 18$ MeV at T=0. The $T\tau lnA$ term is a term introduced by Fisher to account for the power law fall-off of yield distributions at a critical point with τ a critical exponent. The probability of forming a drop of A nucleons is $P \propto \exp(-\Delta G/T)$ where $\Delta G = G_{withdrop} - G_{nodrop}$. This gives a cluster distribution $N(A)$, to a constant C,

$$N(A) = \frac{C}{A^\tau} \exp[\frac{\mu_g - \mu_l}{T} A - \frac{4\pi R^2 \sigma}{T} A^{2/3}] \tag{20.1}$$

On the coexistence curve of a liquid-gas phase transition $\mu_g = \mu_l$ and $N(A)$ is a monotonically decreasing function of A. For a supersaturated system $\mu_g > \mu_l$ and $N(A)$ has a minimum value at a critical size droplet A_c. Neglecting the τlnA term, A_c is given by $A_c^{1/3} = \frac{2}{3} \frac{4\pi r_0^2 \sigma}{\mu_g - \mu_l}$.

The model fits yields of many heavy-ion collisions.

XXI. ISOSPIN FRACTIONATION IN MEAN-FIELD THEORY

Early studies of the liquid-gas phase transition were carried out using a Skyrme interaction and focussed mostly on a one component system made of nucleons even though expressions were developed for two component system of protons and neutrons [12]. The one component aspects are given in section II of this review. The two component aspects will now be discussed in a mean-field approach with this section based mostly on the work of Muller and Serot [107]. Extensions of the results of [12] are now being carried out in [149] using a Skyrme interaction while the Muller-Serot analysis is based on a relativistic mean-field model. Initial results in [149] are qualitatively similar to those of [107]. Both approaches allow a complete calculation various thermodynamic properties, such as the pressure and proton and neutron chemical potentials. In one component systems, the Skyrme interaction and the relativistic mean-field model lead to an S-shaped behaviour of pressure versus volume or density at fixed temperature with stable, unstable, supersaturated and supercooled regions. The standard Maxwell construction describes the liquid to gas phase transition with both phases having the same pressure $p_L = p_G$, and the chemical potential $\mu_L = \mu_G$. The equality of chemical potentials of the liquid and gas phases in phase equilibrium is equivalent to equal areas of the regions above and below the Maxwell or vapour pressure line in the S-shaped loop in p vs. V. For two component systems, phase equilibrium becomes more complicated since the proton to neutron ratio can be different in the two phases because of the symmetry energy which favours $N = Z$. Since the symmetry energy will be large in the denser liquid phase, the proton-neutron asymmetry will be bigger in the gas phase than in the liquid phase. In two component systems, the phase equilibrium conditions consist of

setting, at fixed pressure, the proton chemical potentials in the two phases equal to each other and similarly, the neutron chemical potentials are equal in the liquid and gas phases. The properties of the phase separation boundaries (binodals) and instability boundaries (spinodals) are studied as a function of a quantity labelled $y = \rho_p/\rho$ which is the proton fraction, with the neutron fraction given as $\rho_n/\rho = 1 - y$, and $\rho = \rho_n + \rho_p$. For two component systems, the binodals are now a surface in plots in (p, T, y) space. By contrast, for one component systems, the binodal is a line for the vapour or Maxwell pressure vs. T which terminates at the critical temperature $T = T_c$. The line is at $y = 0.5$ in the (p, T, y) space of two component systems. The two dimensional binodal surface of the phase coexistence boundary now contains a line of critical points for different values of y and a line of maximal asymmetry. In a (p, T, y) plot of the binodal surface, the intersection of a fixed T plane with the surface gives a loop of p vs. y. The maximal asymmetry point is at $(dy/dp)_T = 0$ and physically corresponds to the smallest proton ratio or the largest neutron ratio on the binodal surface at each T. The critical point is at $(dp/dy)_T = 0$ on this loop. The loop degenerates to a point at the critical temperature of a symmetric system $y = 0.5$ (see fig. 7 in [107]). If T and p are both fixed, the binodal surface has two values of y: $y_1(T, p)$ and $y_2(T, p)$ corresponding to different values of the proton fraction in the liquid and gas phase. These different values arise because of the difference in symmetry energy in the liquid and the gas phase. One of the interesting conclusions of the mean-field two component model of the liquid-gas phase transition is that the first-order transition of a one component system becomes a second-order transition. Because of the greater dimensionality in the physical situation, the phase transition is continuous. The role of dimensionality due to the number of components of the system on the order of the phase transition was also pointed out by Glendenning [150].

XXII. DYNAMICAL MODELS FOR FRAGMENTATION

The one common characteristic of all the theoretical models considered so far is that they are static, i.e., they all assume that equilibrium is achieved and hence laws of eqiulibrium statistical mechanics apply. A more fundamental calculation would use a transport equation. Here two nuclei approach each other in their ground state. By solving a time dependent equation we see what the final outcomes are.

The BUU model does start with two nuclei, in their ground states, boosted towards each other. One does not have to introduce a temperature. The model has a mean-field as well as hard collisions and has indeed proven to be highly successful in predicting sideward flow, squeeze-out etc. [56]. While BUU is good for predicting expectation values of one-body operators, it does not have fluctuations. Thus it will not produce clusters. A great deal of effort went into introducing fluctuations in BUU type formalism. A very short list of references are [151–155]. Unfortunately, practical calculations are extremely time consuming. In rare cases calculations have been done to compare with experimental data [156] but the method has not been pushed to see, for example, the rise and fall of IMF production, an accurate estimation of the τ parameter etc. Maybe, in future such calculations will be done.

While exact calculations for heavy-ion collisions based on quantum mechanics are impossible to carry out, classical calculations for ion-on-ion collisions for $\approx$400 particles are entirely feasible with present day computers. This requires solving for each particle i : $d\vec{r}_i/dt = \vec{p}_i/m$

and $d\vec{p}_i/dt = -\sum_{j\neq i} \vec{\nabla}_{r_i} V(\vec{r}_i, \vec{r}_j)$. Here $V(\vec{r}_i, \vec{r}_j)$ is the two body interaction. One starts at time $t = 0$ with initial values of $\vec{r}_i, \vec{p}_i$ and numerically integrates out time. In a set of three papers [157–159] Pandharipande and coworkers studied disassembly of hot classical drops as well as collisions between cold charged argon balls containing A_1 and A_2 particles. The chosen values of (A_1, A_2) were (108,108), (200,16) and (65,65) [157]. The interaction between atoms was a truncated (12,6) potential and a Coulomb interaction was added. Although this is thirteen years later, the reader will find reference [157] still very relevant and revealing. As a function of time, the evolution of temperature and density of the central region is plotted so that one can see under what initial conditions the central region reaches spinodal instability and what the final products are in such cases. They point out that the mass yields calculated in the disassembly of hot equilibrated drops having 216 particles and density somewhat less than normal density is very similar to mass yield of 108+108 collisions. Thus the assumption of statistical equilibrium is valid. The authors stress that the classical argon balls used in the study are not intended to be mock nuclei, but instead to provide simple systems whose time evolution can be studied exactly by solving Newton's equations of motion. Direct comparisons with nuclear data are difficult. Nonetheless, there are many similarities. A power law for fragment yields followed from these calculations, the minimum value being about 1.7. Another remarkable feature is that the apparent temperature deduced from the fragment kinetic energies is much larger than that of the system. The large kinetic energies of fragments in the simulation appear to come from collective motion of expansion and Coulomb repulsion.

In a later paper, the Illinois group devised a simple nucleon-nucleon potential for classical calculations of nuclear heavy ion collisions [160]. They did not use this potential to study liquid-gas phase transition but instead used this at Bevalac energies to investigate flow angles and transverse momenta. Later, disassembly of a collection of nucleons which start with initial temperature and density of interest in this article, and interact via this potential was considered by other groups [161–164]. Pratt et al. [165] used a truncated (8,4) potential to study similar dissociation. It has not been demonstrated that such simulations apply to nuclear cases very well since actual nuclear data for specific cases have not been compared.

The Frankfurt group proposed a simulation which they called quantum molecular dynamics(QMD). This was used for Bevalac energies initially. Relativistic versions exist and are in frequent use. This has also been used for energy region of interest here. Detailed exposition of the model exists [166]. Here each nucleon is represented by a Gaussian in coordinate and momentum space with widths consistent with uncertainty principle. The centroids of the Gaussians move but the widths are kept fixed. The centroids move under the influence of mean-field except when the centroids move very close to each other ($b < \sqrt{\sigma/\pi}$). Then they scatter as in two-body scattering. Pauli blocking is taken into account for scattering. Because each particle is represented by a centroid in phase space with fixed widths in momentum and coorinate space, there is fluctuation built into the system and in the final stage one can recognise clusters. In calculations reported in reference [84] fragment multiplicities were underpredicted in the energy region of interest here. The Copenhagen group has done simulations using a prescription which they dubbed nuclear molecular dynamics [167]. This is quite similar to QMD.

All such simulations which provide clusters at the end are quite computer intensive.. The clusters are easily recognised if each event is run until "asymptotic" times so that different

clusters are well separated from each other. But that requires considerable computer time. Quite sophisticated algorithms have been introduced for early recognition of clusters [168]. This is of practical importance.

Many other models are on the market which will simulate ion-on-ion collisions. They were not necessarily introduced to study liquid-gas phase transition. Some references are [169–171]. Phase transition aspects were discussed in reference [172].

A very attractive model, expanding emitting source (EES) model was proposed by Friedman [173]. This model assumes that initially the hot system evaporates as well as expands. For low initial temperature the system will cease expanding and will revert towards normal density. But beyond a certain temperature at the end of this slow expansion the system will explode. The relationship of this model to liquid-gas phase transition will be interesting to explore.

XXIII. OUTLOOK

The possible links of many experimental observables to expected liquid-gas phase transition in finite nuclear systems continue to be a fascinating story. Much has been learnt and much remains to be learnt. The topic has forced nuclear physicists to delve into realms that were not familiar to them. Necessity has prompted us to do interesting theoretical work, for example, [145] in finite-size scaling and in general, about phase transitions in "small" systems [174]. We are exploring ideas which are of relevance in other fields. There is a broadening of the horizon which is refreshing. We foresee substantial effort in several directions, for example, in dynamical models.

Just fifteen years ago, multifragmentation was barely mentioned in the literature. However, in the past decade tremendous progress has been made in understanding the multifragmentation process and its relationship to the liquid-gas phase transition in nuclear matter. Even though we have not found one definitive experimental signature pinpointing the phenomenon, we know that a mixed phase can be created in the heavy-ion reactions, that multifragmentation occurs within 50-200 fm/c after the initial collisions with a freeze-out density of less than 1/3 of the normal nuclear density, and that the freeze-out temperature is probably in the range of 4-6 MeV. In the near future, experiments will be designed to measure excitation energy, reaction time and freeze-out densities and other observables more precisely. Nonetheless, the availability of comprehensive experimental data has stimulated intense interest on the theoretical front leading to better understanding of the statistical and dynamical nature of nuclear collisions. More exciting developments will be awaiting in the exploration of the isospin degree of freedom in the liquid-gas phase transition with the availability of high to moderate intensity radioactive beams.

In writing this article we have also realised that a vast amount of work has been done in this field by groups widely spread geographically. The literature on this subject is colossal. Our reporting had to be necessarily selective, influenced largely by our own involvement and experience. We are particularly aware that in writing an article about a subject whose scope is this large we must have left out a significant amount of interesting work. For example, several review articles can be written on the subject matter of the last section alone. We finish therefore by apologising for all the omissions that occurred.

XXIV. ACKNOWLEDGEMENTS

Subal Das Gupta thanks J. Lopez for an advanced copy of a monograph on heavy-ion collision reactions written by Lopez and Dorso [175]. Research support was provided by Natural Sciences and Engineering Research Council, *le Fonds pour la Formation de Chercheurs et l'aide à la Recherche du Québec*, the National Science Foundation Grant No. PHY-95-28844 and the U.S. Department of Energy Grant No. DE FG02-96ER40987.

REFERENCES

[1] P. Ring and P. Schuck, *The Nuclear Many-Body Problem* (Springer-Verlag, New York, 1980), Chap. 5

[2] H. Jaqaman, A. Z. Mekjian and L. Zamick, Phys. Rev **C27**, 2782 (1983)

[3] F. Reif, *Fundamentals of statistical and thermal physics*(McGraw Hill, New York, 1965), chap. 8

[4] P. J. Siemens, Nature, **305**, 410 (1983)

[5] M. W. Curtin, H. Toki, and D. K. Scott, Phys. Lett **B123**, 289 (1983)

[6] G. F. Bertsch and P. J. Siemens, Phys. Lett. **B126**, 9 (1983)

[7] W. A. Friedman and W. G. Lynch, Phys. Rev **C28**, 16 (1983).

[8] V. F. Weisskopf, Phys. Rev. **52**, 295 (1937)

[9] S. Das Gupta and G. D. Westfall, Physics Today, May, 34 (1993)

[10] J. Pochodzalla *et.al*, Phys. Rev. Lett **75**, 1040 (1995)

[11] P. Heller, Rep. Prog. Phys. **30**, 731 (1967)[see p. 785]

[12] H. R. Jaqaman, A. Z. Mekjian and L. Zamick, Phys. Rev **C29**, 2067 (1984)

[13] K. Huang,*Statistical Mechanics*(John Wiley and Sons, New York, 1987), chap. 14

[14] J. N. De, S. Das Gupta, S. Shlomo, and S. K. Samaddar, Phys. Rev **C55**, R1641 (1997)

[15] A. M. Poskanzer et. al. Phys. Rev **C3**, 882 (1971)

[16] G. D. Westfall et. al., Phys. Rev **C17**, 1368 (1978)

[17] J. E. Finn et.al., Phys. Rev. Lett. **49**, 1321 (1982)

[18] A. S. Hirsch et. al., Phys. Rev. **C29**, 508 (1984)

[19] D. J. Fields, W. G. Lynch, C. B. Chitwood, C. K. Gelbke, M. B. Tsang, H. Utsunomiya, J. Aichelin, Phys. Rev **C30**, 1912 (1984)

[20] L. G. Sobotka et. al. Phys. Rev. Lett. **51**, 2187 (1983)

[21] L. Phair et. al. Nucl. Phys. **A548**, 489 (1992)

[22] G. J. Kunde et. al. Phys. Rev **C55**, R990 (1997)

[23] L. Phair et. al. Phys. Rev **C60**, 054617 (1999)

[24] W. J. Llope et. al. Phys. Rev **C51**, 1325 (1995)

[25] J. Lukasik et. al. Phys. Rev **C55**, 1906 (1997)

[26] C. Cavata, M. Demoulins, J. Gosset, M-C Lemaire, D. L'Hôte, J Poitou, O. Valette, Phys. Rev **C42**, 1760 (1990)

[27] C. Williams, Ph. D. thesis, Michigan State University, (1998)

[28] L. Phair et. al. Nucl. Phys. **A564**, 453 (1993)

[29] M. D'Agostino et. al. Phys. Rev. Lett. **75**, 4373 (1995)

[30] H. S. Xu et. al. Phys. Rev. Lett. **85**, 716 (2000)

[31] P. Danielewicz, Phys. Rev **C51**, 716 (1995)

[32] W. Reisdorf and H. G. Ritter, Ann. Rev. of Nucl. Part. Sci **47**, 553 (1997)

[33] J. F. Dempsey et. al. Phys. Rev **C54**, 1710 (1996)

[34] J. Hubele et. al. Z. Phys. **A340**, 263 (1991)

[35] W. C. Hsi, Ph. D. thesis, Michigan State University, 1995

[36] K. Tso et. al. Phys. Lett. **B361**, 25 (1995)

[37] D. R. Bowman et. al. Phys. Rev. Lett. **67**, 1527 (1991)

[38] W. C. Hsi et. al. Phys. Rev. Lett. **73**, 3367 (1994)

[39] M. A. Lisa et. al. Phys. Rev. Lett. **75**, 2662 (1995)

[40] C. Williams et. al. Phys. Rev **C55**, R2132 (1997)

[41] J. Lauret et. al. Phys. Rev **C57**, R1051 (1998)
[42] M. D'Agostino et. al. Phys. Lett. **B371**, 175 (1996)
[43] R. Hanbury-Brown and R. Q. Twiss, Nature **178**, 1046 (1956)
[44] D. Fox et. al. Phys. Rev. **C47**, R421 (1993)
[45] T. Glasmacher et. al. Phys. Rev **C50**, 952 (1994)
[46] D. Durand et. al. Phys. Lett. **B345**, 297 (1995)
[47] E. Bauge et. al. Phys. Rev. Lett. **70**, 24 (1993)
[48] L. Beaulieu et. al. Phys. Rev. Lett. **84**, 5971 (2000)
[49] S. Pratt, Nucl. Phys. **A638**, 125 (1998)
[50] F. Zhu et. al. Phys. Rev. **C44**, R582 (1991)
[51] S. Fritz et. al. Phys. Lett. **B461**, 315 (1999)
[52] J. Hubele et. al. Phys. Rev. **C46**, R1577 (1992)
[53] K. Hagel et. al. Phys. Rev. **C50**, 2017 (1994)
[54] A. S. Botvina et. al. Nucl. Phys. **A584**, 737 (1995)
[55] J. Cugnon, T. Mizubani, and J. Vandermeulen, Nucl. Phys. **A352**, 505 (1981)
[56] G. F. Bertsch and S. Das Gupta, Phys. Rep. **160**, 189 (1988)
[57] T. K. Nayak et. al. Phys. Rev. **C45**, 132 (1992)
[58] W. Bauer, Phys. Rev. **C51**, 803 (1995)
[59] C. Schwarz et. al. Phys. Rev **C48**, 676 (1993)
[60] H. Xi, W. G. Lynch, M. B. Tsang, W. A. Friedman and D. Durand, Phys. Rev **C59**, 1567 (1999)
[61] S. Albergo et. al. Nuovo Cimento **A89**, 1 (1985)
[62] J. Pochodzalla et. al. Phys. Lett. **B161**, 275 (1985)
[63] M. B. Tsang, W. G. Lynch, H. Xi and W. A. Friedman, Phys. Rev. Lett. **78**, 3836 (1997)
[64] M. B. Tsang et. al. Phys. Rev **C53**, R1057 (1996)
[65] H. Xi et. al. Phys. Rev **C57**, R467 (1998)
[66] V. E. Viola, K. Kwiatkowski and W. A. Friedman, Phys. Rev **C59**, 2660 (1999)
[67] J. A. Hauger et. al. Phys. Rev **C62**, 24616 (2000)
[68] H. Xi et. al. Phys. Lett. **B431**, 8 (1998)
[69] S. R. Souza et. al. Phys. RevC. (in press)
[70] M. J. Huang et. al. Phys. Rev. Lett. **78**, 1648 (1997)
[71] V. Serfling et. al. Phys. Rev. Lett. **80**, 3928 (1998)
[72] D. Durand, Nucl. phys. **A630**, 52 (1998)
[73] H. F. Xi et. al. Phys. Rev **C58**, R2636 (1998)
[74] C. B. Chitwood et. al. Phys. Rev. **C34**, 858 (1986)
[75] H. F. Xi, private communication.
[76] C. K. Gelbke, private communication.
[77] Z. Chen et. al., Phys. Rev. **C36**, 2297 (1987)
[78] J. A. Hauger et. al. , Phys. Rev **C57**, 764 (1998)
[79] L. Beaulieu et. al. , Phys. Lett. **B463**, 159 (1999)
[80] M. D'Agostino et. al., Phys. Lett. **B473**, 219 (2000)
[81] J. B. Natowitz et. al.,Phys. Rev **C52**, 2322 (1995)
[82] G. F. Peaslee et. al., Phys. Rev **C49**, R2271 (1994)
[83] C. A. Ogilvie et. al. Phys. Rev. Lett. **67**, 1214 (1991)

[84] M. B. Tsang et. al., Phys. Rev. Lett. **71**, 1502 (1993)
[85] M. E. Fisher, Physics, **3**, 255 (1967)
[86] J. Hufner and D. Mukhopadhyay, Phys. Lett. **B173**, 373 (1986)
[87] L. Oddershede, P. Dimon and J. Bohr, Phys. Rev. Lett. **71**, 3107 (1993)
[88] J. Pan and S. Das Gupta, Phys. Lett. **B344**, 29 (1995)
[89] J. Pan and S. Das Gupta, Phys. Rev **C51**, 1384 (1995)
[90] M. L. Gilkes et. al., Phys. Rev. Lett. **73**, 1590 (1994)
[91] W. Bauer and A. Botvina, Phys. Rev. **C52**, R1760 (1995)
[92] X. Campi and J. Debois, in Proceedings of the Seventh High Energy Heavy Ion Study, GSI Darmstadt, 1984, GSI Report No 85-10, 1985, p 707
[93] W. Bauer, D. R. Dean, U. Mosel, and U. Post, in Proceedings of the Seventh High Energy Heavy Ion Study, GSI Darmstadt, 1984, GSI Report No 85-10, p 701
[94] X. Campi, Phys. Lett **B208**, 351 (1988)
[95] W. Bauer, Phys. Rev **C38**, 1297 (1988)
[96] D. Stauffer and A. Aharony, *Introduction to Percolation Theory*, (Taylor and Francis, London, 1992)
[97] S. Das Gupta, J. Pan, J. Kvasnikova, and C. Gale, Nucl Phys. **A621**, 897 (1997)
[98] L. P. Csernai and J. I. Kapusta, Phys. Rep. **131**, 223 (1986)
[99] L. G. Moretto et. al. Phys. Rev. Lett. **74**, 1530 (1995)
[100] L. G. Moretto, R. Ghetti, L. Phair, K. Tso, and G. J. Wozniak, Phys. Rev. Lett. **76**, 2822 (1996)
[101] Ph. Chomaz and F. Gulminelli, private communications.
[102] J. P. Bondorf, A. S. Botvina, A. S. Iljinov, I. N. Mishustin, K. Sneppen, Phys. Rep. **257**, 133 (1995)
[103] K. Kwiatkowski et. al. Phys. Lett **B423**, 21 (1998)
[104] J. Cibor et. al. Phys. Lett. **B473**, 29 (2000)
[105] Y. G. Ma et. al. Phys. Lett. **B390**, 41 (1997)
[106] B. A. Li, C. M. Ko, and Z. Ren, Phys. Rev. Lett. **78**, 1644 (1997)
[107] H. Muller and B. D. Serot, Phys. Rev. **C52**, 2072 (1995)
[108] Ph. Chomaz and F. Gulminelli, Phys. Lett **B447**, 221 (1999)
[109] S. K. Samaddar and S. Das Gupta, Phys. Rev. **C61**, 34610 (2000)
[110] Y. G. Ma et. al., Phys. Rev. **C60**, 24607 (1999)
[111] S. J. Yennello, Private Communications.
[112] G. J. Kunde, Private Communications
[113] M. B. Tsang, W. A. Friedman, C. K. Gelbke, W. G. Lynch, G. Verde and H. Xu, to be published.
[114] V. Baran, M. Colonna, M. Di Toro and A. B. Larionov, Nucl. Phys. **A632**, 287 (1998)
[115] D. H. E. Gross, Phys. Rep. **279**, 119 (1997)
[116] J. Randrup and S. E. Koonin, Nucl. Phys. **A471**, 355c (1987)
[117] A. H. Raduta and A. R. Raduta, Phys. Rev **c55**, 1344 (1997)
[118] A. Z. Mekjian, Phys. Rev. Lett. **38**, 640 (1977)
[119] B. K. Jennings and S. Das Gupta, Phys. Rev. **C62**, 14901 (2000)
[120] K. C. Chase and A. Z. Mekjian, Phys. Rev. **C50**, 2078 (1994), Phys. Rev. **C49**, 2164 (1994)
[121] S. Das Gupta and A. Z. Mekjian, Phys. Rev. **C57**, 1361 (1998)

[122] D. Hahn and H. Stocker, Nucl. Phys. **A452**, 723 (1986)
[123] A. Majumder and S. Das Gupta, Phys. Rev **C59**, 845 (1999)
[124] J. B. Elliott and A. S. Hirsch, Phys. Rev. **C61**, 54605 (2000)
[125] K. A. Bugaev, M. I. Gorenstein, I. N. Mishustin and W. Greiner, arXiv:nucl-th/0005036, 14 May, 2000
[126] J. P. Bondorf, R. Donangelo, I. M. Mishustin, C. J. Pethik, H. Schulz and K. Sneppen, Nucl. Phys. **A443**, 321 (1985)
[127] P. Bhattacharyya, S. Das Gupta and A. Z. Mekjian, Phys. Rev. **C60**, 54616 (1999)
[128] P. Bhattacharyya, S. Das Gupta and A. Z. Mekjian, Phys. Rev **C60**, 64625 (1999)
[129] A. Majumder and S. Das Gupta, Phys. Rev **C61**, 34603, (2000)
[130] H. M. Xu et. al. Phys. Rev **C40**, 186 (1989)
[131] J. P. Bondorf, R. Donangelo, I. M. Mishustin and H. Schulz, Nucl. Phys. **A444**, 460 1985
[132] K. Sneppen, Nucl. Phys. **A470**, 213 (1987)
[133] D. H. E. Gross and H. Massmann, Nucl. Phys. **A471**, 3339c (1987)
[134] M. P. Allen and D. J. Tildesley, *Computer Simulation of Liquids*(Oxford University Press, New York,1996), chapter 4.
[135] N. Metropolis, A. W. Rosenbluth, M. N. Rosenbluth, A. H. Teller, and E. Teller, J. Chem. Phys. **21**, 1087 (1953)
[136] T. D. Lee and C. N. Yang, Phys. Rev **87**, 404 (1952)
[137] X. Campi and H. Krivine, Nucl. Phys. **A620**, 46 (1997)
[138] S. Das Gupta and J. Pan, Phys. Rev **C53**, 1319 (1996)
[139] T. S. Biro, J. Knoll and J. Richert, Nucl. Phys. **A459**, 692 (1986)
[140] A. Coniglio and W. Klein, J. of Phys. **A13**, 2775 (1980)
[141] J. Kertész, Physica, **A161**, 58 (1989).
[142] J. Pan, S. Das Gupta and M. Grant, Phys. Rev. Lett. **80**, 1182 (1998)
[143] W. D. Myers and W. J. Swiatecki, Nucl. Phys. **81**, 1 (1966)
[144] J. Pan and S. Das Gupta, Phys. Rev **C57**, 1839 (1998)
[145] F. Gulminelli and Ph. Chomaz, Phys. Rev. Lett. **82**, 1402 (1999)
[146] J. Borg, I. N. Mishustin and J. P. Bondorf, Phys. Lett. **B470**, 13 (1999)
[147] Y. G. Ma, Phys. Rev. Lett. **83**, 3617 (1999)
[148] A. L. Goodman, J. I. Kapusta and A. Z. Mekjian, Phys. Rev. **C30**, 851 (1984)
[149] S. J. Lee and A. Z. Mekjian, to be published.
[150] N. K. Glendenning, Phys. Rev. **D46**, 1274 (1992)
[151] C. Gale and S. Das Gupta, Phys. Lett **162B**, 35 (1985)
[152] W. Bauer, G. F. Bertsch and S. Das Gupta, Phys. Rev. Lett. **58**, 863 (1987)
[153] S. Ayik and C. Gregoire, Phys. Lett **B212**, 269 (1988)
[154] S. Ayik and C. Gregoire, Nucl Phys. **A513**, 187 (1990)
[155] G. F. Burgio, Ph. Chomaz and J. Randrup, Nucl. Phys. **A529**, 157 (1991)
[156] J. Gallego et. al. Phys. Rev **C44**, 463 (1991)
[157] T. J. Schlagel and V. R. Pandharipande, Phys. Rev. **C36**, 162 (1987)
[158] R. J. Lenk and V. R. Pandharipande, Phys. Rev. **C34**, 177 (1986)
[159] A. Vicentini, G. Jacucci and V. R. Pandharipande, Phys. Rev. **C31**, 1783 (1985)
[160] R. J. Lenk, T. J. Schlagel and V. R. Pandharipande, Phys. Rev. **C42**, 372 (1990).
[161] V. Latora, M. Belkacem and A. Bonasera, Phys. Rev. Lett. **73**, 1765 (1994)

[162] M. Belkacem, V. Latora and A. Bonasera; Phys. Rev. **C52**, 271 (1995)
[163] P. Fonocchiaro, M. Belkacem, T. Kubo, V. Latora and A. Bonasera, Nucl. Phys. **A600**, 236 (1996)
[164] C. O. Dorso, V. C. Latora and A. Bonasera, Phys. Rev. **C60**, 34606 (1999).
[165] S. Pratt, C. Montoya and F. Ronning, Phys. Lett. **B314**, 261 (1995)
[166] J. Aichelin, Phys. Reports **202**, 233 (1991)
[167] J. P. Bondorf, D. Idier and I. N. Mishustin, Phys. Lett. **B359**, 261 (1995)
[168] A. Strachan and C. O. Dorso, Phys. Rev. **C55**, 775 (1997)
[169] D. H. Boal and J. N. Glosli, Phys. Rev. **C42**, 502 (1990)
[170] H. Feldmeier, K. Bieler and J. Schnack, Nucl. Phys. **A586**, 493 (1995)
[171] A. Ono, H. Horiuchi, and T. Maruyama, Phys. Rev. **C48**, 2946 (1993)
[172] J. Schnack and H. Feldmeier, Phys. Lett. **B409**, 6 (1997)
[173] W. A. Friedman, Phys. Rev. **C42**, 667 (1990)
[174] D. H. E. Gross and E. V. Votyakov, Eur. Phys. J. **B15**, 115 (2000)
[175] J. A. Lopez and C. O. Dorso, *Lecture notes on Phase Transformation in Nuclear Matter: the liquid-gas phase transition* (to be published by World Scientific) .